Sequenced Somatic Cell Reprogramming and Differentiation Inside Nested Hydrogel Droplets

Green, David W; Watson, Jolanta A; Watson, Gregory S; Stamboulis, Artemis

Link to publication on Research at Birmingham portal

Sequenced Somatic Cell Reprogramming and Differentiation Inside Nested Hydrogel Droplets

David W. Green,* Jolanta A. Watson, Gregory S. Watson, and Artemis Stamboulis

The efficient genesis of pluripotent cells or therapeutic cells for regenerative medicine involves several external manipulations and conditioning protocols, which drives down clinical applicability. Automated programming of the genesis by microscale physical forces and chronological biochemistry can increase clinical success. The design and fabrication of nested polysaccharide droplets (millimeter-sized) with cell sustaining properties of natural tissues and intrinsic properties for time and space evolution of cell transformation signals between somatic cells, pluripotent cells and differentiated therapeutic cells in a swift and efficient manner without the need for laborious external manipulation are reported. Cells transform between phenotypic states by having single and double nested droplets constituted with extracellular matrix proteins and reprogramming, and differentiation factors infused chronologically across the droplet space. The cell transformation into germ layer cells and bone cells is successfully tested in vitro and in vivo and promotes the formation of new bone tissues. Thus, nested droplets with BMP-2 loaded guests synthesize mineralized bone tissue plates along the length of a cranial non-union bone defect at 4 weeks. The advantages of sequenced somatic cell reprogramming and differentiation inside an individual hydrogel module without external manipulation, promoted by formulating tissue mimetic physical, mechanical, and chemical microenvironments are shown.

1. Introduction

Therapeutic cells are replacements for damaged, dysfunctional, and previously destroyed cells within tissues and organs of patients. For total clinical success, the cells must originate

from the patient. The cells would then be safer and not cause immune responses. The most promising cells for human cell and tissue therapy are Human embryonic stem cells (hESC's), human pluripotent cells (hPC's), and embryonic-like human induced pluripotent stem cells (hiPSC's). This is because they indefinitely divide into new stem cells, and they can transform into many other phenotypes, given the right conditions.[1,2]

Using healthy patient's cells from skin or fat tissues requires hard technical skills in transforming cell phenotypes between different and disparate specialized phenotypes. The best practice is to create pluripotent cell phenotypes. Clinical success is guaranteed when the cells originate from the patient. Effective cell therapy requires technical skills in transforming cell identities between different and disparate specialties. The best practice is to create pluripotent cell phenotypes that can generate very large populations.[3–5]

PSC's possess an inordinate capacity to generate any of the approximately 200 different specialized cell types. This is achieved through the fine-scale modulation of biochemical, physical,[6–8] mechanical, and material permutations.[2] These highly potent PSCs provide the best possible among any cell type to generate multiple billions of cells for every patient.[3]

Simple, fast, scalable and highly efficient methods of cell reprogramming and differentiation into billions of stable therapeutic cells are essential for sizeable tissue substitutions or large-scale physiological restoration in regenerative medicine.[3–5] However, reprogramming protocols are the use of integrating or nonintegrating vectors.[9,10] Invariably, the current methods, which are based predominantly on gene integration, frequently use viral vectors. This, despite their perfectly adapted ability to lead to low transformation efficiencies typically between 0.01 and 1% and a maximum of up to 7%.[11–13] The production of PSCs with extraordinary rates of efficiency, leading to increased yields is vital to generate clinically relevant tissue volumes.

There are reports of reprogramming rates of 30%. Replanting the freshly reprogrammed cells on laminin coated surfaces increases the level pluripotency to 80% within a fibroblast population. That is after a spell of continuous culture for 14 days on VTN-coated substrates. On this theme, the treatment of fibroblasts with recombinant proteins coded by Yamanaka transcription factors dramatically increased reprogramming to

Dr. D. W. Green, Dr. A. Stamboulis
School of Metallurgy and Materials, Healthcare Technologies Institute
University of Birmingham
Edgbaston, Birmingham B15 2TT, UK
E-mail: d.w.green.1@bham.ac.uk

Dr. J. A. Watson, Dr. G. S. Watson
School of Science and Engineering
University of the Sunshine Coast
Fraser Coast, Hervey Bay, QLD 4655, Australia

The ORCID identification number(s) for the author(s) of this article can be found under https://doi.org/10.1002/adbi.202000071.

ADVANCED
SCIENCE NEWS

www.advancedsciencenews.com

ADVANCED
BIOSYSTEMS

www.adv-biosys.com

above 80%.[14] However, there is a spectrum of natural forces in the tissues that reinforce cell reprogramming and onward differentiation and make it more controlled and flexible. So far, the PSC culture methods do not apply a suitable balance of biochemical, physical, and mechanical forces. Some clues to the identification of the other forces involved in natural cell reprogramming and differentiation can be found in the early embryo (inner cell mass (ICM) of the blastocyst)[15,16] For instance, the matrix in the ICM is rich in collagen IV, Laminins and E-cadherins.[2,17] Structural biomaterials are able to apply all these forces on cells and force changes into a spectrum of phenotypes. Already, biomaterials have been used to support and boost cell reprogramming and force differentiation.

Biomaterial frameworks with cells can significantly enhance the reprogramming of hESC's and human pluripotent stem cells (hPSC's) by combining important forces from physics and chemistry.[18] A wide range of structural biomaterials differentiate embedded stem cells, and far fewer actually reprogram.[19] Biomaterials with hierarchical structure and stiffness encourage stem cell specialisations[20,21] a specially reconditioned natural extracellular matrix (ECM) derivative, Matrigel; high water contents and changeable structures to encourage stem growth and then differentiation,[22,23] specifically well-honed polyethylene glycol (PEG) hydrogel with protein for swift stem cell specialisation,[24] and biomaterials that support differentiated cell "engraftment" and interaction with the immune system for efficient repair.[25] In effect biological ceramics, and natural and synthetic polymers have in one way or another influenced stem cell differentiation and occasionally reprogramming.

Biomaterial frameworks have also encouraged the differentiation of 3D arranged the embedded hESC's and hiPSC's into functional tissue derived from 50–80% of the original PSC population.[26] For example, hESC's embedded in gels of alginate-extracellular matrix proteins (ECMp) (2–5%). Hydrogels of hyaluronic acid give further examples of the extraordinary influence on ESC and PSC proliferation and differentiation Poly-L-lactic acid (PLLA)/poly-glycolic acid (PLGA), Matrigel, each possesses the capacity to choreograph cartilage, endothelial tubules, neurons, and hepatocytes.[27–29]

Innovative solutions to the problem focus on the spatial and temporal separation of the defining factors in cell transformations.[30] Precisely targeting the individual cell with transcription factors, functional gene sequences, small proteins, and chemically defined small molecules is a prominent role for dynamic, information-rich biological materials and their structures.[8,31] These frame the cell by actual spatial positioning, signal to sequence, and follow the natural course of molecular and physiological events. Cell encapsulation within structured biomaterials provides a capable vehicle for transplantation.[30] The vehicles concentrate therapeutic cells at the final implanted location, facilitating integration and assimilation with the host.[32] Physical, mechanical, and architectural properties of the microenvironment convert cells at high rates and efficiencies. These dynamics require temporal separation reprogramming and differentiation factors (DF's).[6,33] And finally, there is the requirement for accurate sequencing of the various forces and biochemicals to re-enact the appropriate changes in cell phenotypes.[34]

The major problem of applying pluripotent stem cells to therapeutic roles is a) properly controlling their production

from somatic cells in large numbers and b) their terminal differentiation into specialized cells. The use of biomaterials is paramount in carrying out the controlled reprogramming and differentiation of both somatic cells and pluripotent cells in 3D arrangements. This is because biomaterials add mechanical and physical forces to the cells in nature, realistic 3D arrangements. The objective is to mimic cells in the ECM and provide a time and space evolution and chronology that autonomously converts somatic cells between pluripotent cells and desired therapeutic cell types.

This study follows the design and fabrication of a materials-based biosystem that produces tissue-specific therapeutic cells from fibroblasts without any external manipulation. The nested architecture of polysaccharide droplets supports the fast and effective spatial and temporal delivery of reprogramming and DF in one automatic process. The ECM enriched droplet environment, which partially resembles the ECM content of the ICM, ensures high viability and growth of the transformed cells. Moreover, the mechanical environment and physical confinement in the droplet boosts reprogramming at the outset as reported elsewhere.[18]

2. Results

2.1. Somatic Cell Reprogramming Inside Alginate-ECMp-Chitosan-ECMp mm-Sized Fused Droplets

A small gauged syringe needle manually generated polysaccharide droplets containing cells or differentiation/reprogramming factors. An ionic cross-linking reaction fused the droplets. The encapsulated cells were characterized over the ten-day experiment to observe their transformation in response to i) reprogramming factors and ii) DF's. The schematic shows the principles behind the droplets function, succinctly summarizing the study plan (**Figure 1**A). There is also a timeline for the conversion of a proportion of 80 000–90 000 HDFs within the polysaccharide fused droplets (Figure 1A). Five experimental droplet types were fabricated to correctly determine the likely possibility and feasibility for automation of cell trans-differentiation. This was achieved by providing mm-sized fused droplets either with or without the reprogramming factors (RPFs) and DF's, mm-sized fused droplets (ionically crosslinked) containing mixtures of the RPF and DF's, and nested mm-sized fused droplets containing either one signature cocktail of DF's mixed inside a single guest droplet and for the endoderm induction two guest droplets (Table S1 (Supporting Information), **Table 1**, Experimental Section and Figure 1B1–5). The significant comparisons required to confirm our hypotheses positively were invariably between mm-sized fused droplets, with and without the contributing factors, and between mm-sized fused droplets with comixtures and sequenced delivery of DF's by the nested mm-sized fused droplets.

The producers of the small molecule cocktail and growth factors (Programin human mechanically induced pluripotent stem cells (hmciPSC), Stapworks(R) & StemPro Differentiation kit, R&D Systems) used in this study were prescribed in mM (ranging between 4×10^{-3}–8×10^{-3} м) measurable quantities.
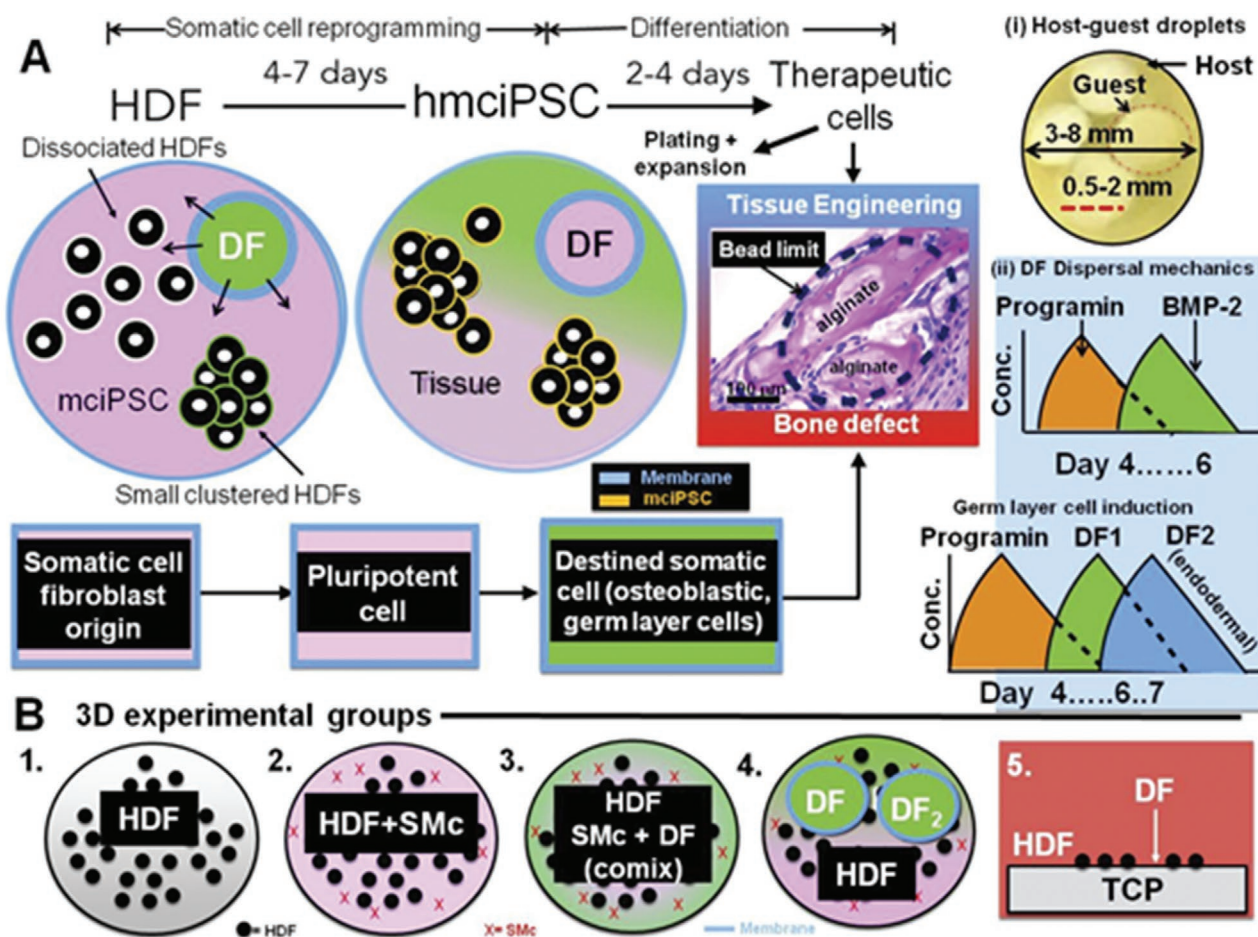
Figure 1. Scheme showing the rational basis for reprogramming and differentiation in alginate droplets. A) A diagram featuring the 3D nested droplet strategy enabling coupling of reprogramming and interconversion between disparate somatic cell lineages: ECMp mm-sized fused droplets and "bead-in-bead" biosystems. The HDF cells are reprogrammed in 3D sequenced to differentiate according to the DF factors incorporated in the guest droplet. Direct use of differentiated cells for therapy runs along two trajectories, 1) plating and expansion for experimentation and cell therapy, and 2) bulk tissue engineering. i) Single and double nested carriers time the mechanism for differentiation for the respective DF's (size ranges of droplets: host diameter = 3–8 mm [14.1–268 mm³]; guest diameters (the red-dotted line) = 0.5–2 mm [0.065–4.1 mm³]); ii) Illustration of the various theorised profiles for the dispersal of regenerative factors (RF) and DF's inside the main droplet where the cells reside. The maximum concentration of RF is at its peak immediately upon cell encapsulation. Following 3–4 days the DF's in the guest droplet is supposed to reach max concentration. Inclusion of a second guest droplet with a thicker, less permeable membrane delays the release of its contents to a peak cell functioning concentration until another 2 days. Four test groups were set up with different encapsulate permutations and the physical structures; B) The main experimental droplet treatments with HDFs to determine the effectiveness of RF and RF+DF timed release. 1) Generated mm-sized fused droplets with HDF's alone inside; 2) HDFs in droplets infused with RF (SMc); 3) Droplets with a comixture of RF and DFs; 4) A static monolayer culture was also prepared 5) with treated Programin (hmciPSC) and DFs on a tissue culture plate (TCP) substrate [Key red × / pink = SM's; black dot = cell; green = DF's].

The commercialized StapWorks(R) product Programin(R) (Stapworks(R)) cocktail represents a creative evolution of the small molecules for reprogramming. A derivative named Rever-

Table 1. Listing of the differentiation factors used to transform mciPSCs into each of the germ layer cell identities.

Endodermal induction factors	Mesodermal induction factors	Ectodermal induction factors
Wnt3	Activin A	Retinoic acid
Activin A	TGFb	EGF
FGF	–	BMP4
–	–	BFGF

sine effectively transdifferentiate fibroblasts into "*skeletal muscle cells*".[14,35] Treatment of HDF cells to Programin (hmciPSC) and DF's in static 2D monolayer cultures occurred at the same time as the bead cultures (Figure 1B5). Most human cells are not fully responsive to clean alginate because it lacks proteins. Therefore, infused in alginate were fibronectin derived Arg-Gly-Asp (cell adhesive tripeptide), liquid RGD (at 0.1 µL mL⁻¹) and extracellular basement membrane proteins, in liquid form to increase cell responsiveness. The ECM proteins used were the same ones enriching the ICM of the pre-implantation blasto-cyst (ICM) and the stem cell niche.[36] Proteins used in alginate included: – laminin, fibronectin, Nanog protein, collagen IV, and chondroitin sulfate.[2,37] The selection of proteins is sup-ported in work by Caiazzo et al.,[18] who augmented PEG gels

with the significant basement membrane protein constituents: laminin, collagen IV and the epithelial cell adhesion molecule, epCAM. These proteins boosted reprogramming efficiencies together with two individual soluble factors, eight ECM proteins, two different degradation properties, and four different levels of stiffness.[18] We confined the alginate to two values of stiffness.

The notable inclusion of ECM engenders the alginate-ECMp active matrix with higher levels of cellular function and activity, and survivability as alginate-ECMp can typically reduce the population by 5% –10%. Analogs of the commonest ICM basement membrane proteins penetrated the alginate nanopores.[17] Proteins provided complex interactions with the matrix resembling the ICM environment. One of the utmost consequences of matrix interactions are to increase naturally the size of small hmciPSC visible clusters (estimated to comprise 70% of the total droplet-based cell population), and the estimated 30% of dissociated hPSC's present in the alginate-ECMp (Figure 1A). Laminin and epCAM stimulated increased tremendously hiPSC generation (Oct-4-green fluorescent protein (GFP) colonies) within 3D PEG gels, compared with the gelatinous ECM (basement membrane complex), Matrigel.[18] Matrices that trigger Wnt signaling pathways and YAP/TAZ should also ostensibly promote pluripotency above normal levels.

2.2. ELB Somatic Cell Reprogramming with Small Molecules Facilitated by a Mechanical Force Field

Inspiration for an alginate-ECMp device supporting cell transformation arose from the adoption of human "mechanically induced" iPSC (hmciPSC) reprogramming methodology. The selected procedure involves seeding 1×10^4 fibroblasts into single 6.4 mm hydrophobic wells. The hydrophobicity creates a mechanical force field that shapes the suspended cells into 500 mm × 400 mm spheroids or embryoid-like bodies (ELB's) (**Figure 2**A). The cells in this collective arrangement are always metabolically active. With each experiment, we confirmed the cell viability through the visible expression of green fluorescent 5-chloromethylfluorescein diacetate (CMFDA; Figure 2B). We carried out this metabolic test eight separate times ($n = 8$ experiments), which totaled 395 wells, generating an equal number of 200 × 400 μm HDF spheroids/ELBs, made from a starting population of 10 000 HDF cells. According to the previous report of the mechanical and chemical induction methodology, the largest size of aggregates that reprogram successfully can be 1×10^6.[38]

Carefully testing the reprogramming and onward differentiation for ourselves, we accurately characterized the cell phenotypes within the spheroids/ELB's immediately after four-days of pluripotency. There was a 23–25.2% conversion rate by manual cell counting of ESC108 positive cells (Figure 2C). ESC108 is a specific marker that does not stain fibroblasts and untreated individual spheroids/ELB's (Figure 2C vs 2C', without SMc treatment control). A broad region of the in situ ELB's stained positively with ESC108 except for the active core, most probably due to the limited diffusion capacity deep inside the ELB, which produces an irregular morphology. Some of the observed diffuse Rhodamine staining and slight image blurring

was the result of explicit image capturing of 3D spheroids/ELBs in situ. The display of the entrapped dye is highlighted in Figure 2D.

Further proof of the hESC bearing phenotype of the reprogrammed cell, spheroid/ELB's were detected by secure UEA-1 lectin (*Ulex europea*) binding, previously identified as a clear and positive hESC identifier.[39] Disclosure of specific lectin binding occurred by fluorescence tagging of the ELB (Figure 2E,E'). A graphic display of E-cadherin labels and Sox-2 labeling of SMc treated and untreated cellular spheroids or ELB is shown in Figure 2F,F'. Such untreated spheroids or ELB's positively stained for the fibroblastic identifying vimentin marker amply demonstrate the absence of "stemness"- the essential characteristics of stem cells from other cells[40] (Figure 2G).

2.2.1. ELB Differentiation

The reprogrammed ELB's are predominantly an aggregate of pluripotent cells, and we examined the propensity of the ELB's to differentiate into either an osteogenic or germ cell layer lineage. ELB's were treated to inductive media invariably containing one of the following morphogens: Activin A, wnt3a, FGF4, TGF-β3, EGF, BMP4 & 7, Retinoic acid, FGF basic (see the Experimental Section). We labeled cells within 4 days for the complementary germ layer marker, Otx2 (Figure 2H), Brachyury (Figure 2I), and Sox17 (Figure 2J). All were positive in marked contrast to the SMc control ELB (Figure 2J') that showed no positive staining with these markers. In notable addition to the local production of tissue progenitor cells, we directly converted the ELB's into a fully committed, specific osteogenic cell lineage. This result emerged from a two-day BMP-2 exogenous media treatment that duly led to osteogenic induction confirmed by 78% positive expression of Osterix (Sp7) and Runx-2 compared with untreated controls. These displayed no direct expression of these reliable markers (Figure 2K,L,L').

2.2.2. ELB Subculture in 2D Monolayers

The mechanical and chemical induction method gently forces the somatic HDF's into spheroids or ELB's for SMc reprogramming. The repulsion to the surface occurs before plating on a growth substrate for population expansion into practically sufficient numbers, as highlighted in Figure 2M–P, instantly following 14 days of monoculture. Again, the untreated spheroids or ELB's seeded onto a 2D monolayer did not stain for specific ESC markers (Figure 2N'), but adequately expressed the definitive fibroblast cell marker, SMA (Figure 2Q). Tracking of the ELB cells for phenotype identification and genome stability was continuous, as these- change following forcible reprogramming. Identifying such changes was achieved by observing their complex morphology and by further immunolabeling for various key hiPSC and hESC markers. These typically included: Nanog, Oct3/4 (Figure 2N), ESC108 (Figure 2O) and Sox-2[38] at day 7 (Figure 2P), in striking contrast to the unprogrammed (the preferential untreated-SMc) ELB/spheroids (Figure 2N').
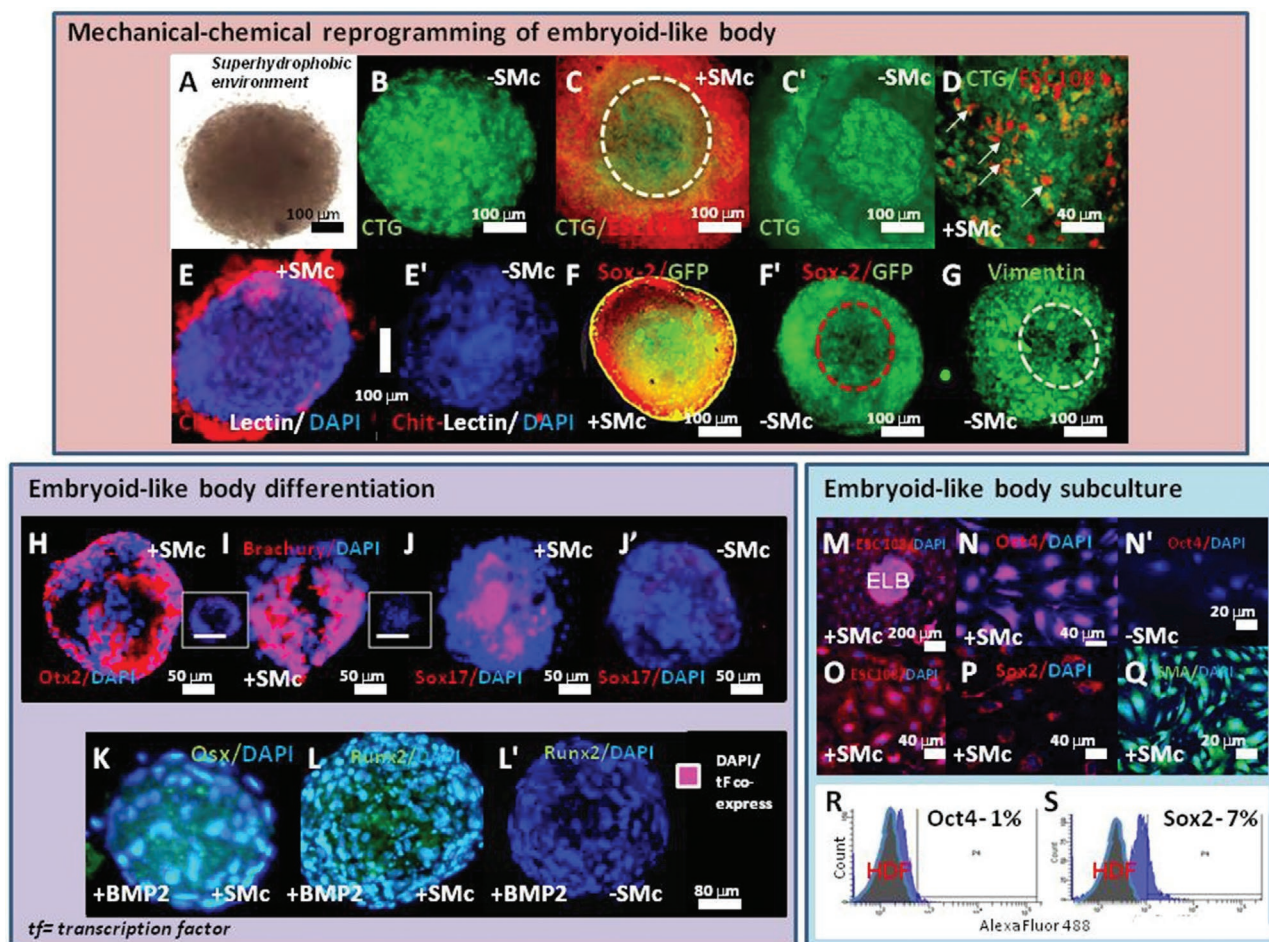
Figure 2. SMc mechanical-chemical reprogramming of nonencapsulated HDF spheroids/ELBs into embryo-like bodies. A) View of an individual HDF cell spheroid under brightfield microscopy at day 2; B) An HDF cell ELB/spheroid at day 4 following full reprogramming expressing for regular metabolic activity GFP to show almost total cell viability (>95%); C) 4-day-old spheroid expressing complementary GFP and ESC (white dotted line encloses the core with reduced cell density); C') A single HDF spheroid was expressing total CTG that was treated to SMc, showing no effect on viability; D) An ELB labeled by CTG and the proprietary ESC-specific dye (ESC108) together, to highlight the simultaneous hmciPSC viability (GFP cell processed dye in green) and pluripotency (red, 25.2%) of the programmed HDFs. The arrows point to positive ESC-like cells; E) A single spheroid/ELB ensheathed by alginate-ECMp-chitosan composite material bound to glycocalyx by ESC defining lectin molecules; E') The parallel control ELB not treated to SMc, but treated to lectin-biotinylated alginate-and Rhodamine infused chitosan; F) Sox-2-positive immunolabeling of a hmciPSC spheroid; (F') SMc untreated spheroid stained with anti-Sox2; G) A single vimentin-positive spheroid/ELB; H) Single ectoderm differentiated cell spheroid with Otx2 expression, particularly around the margins. Inset of ELB not treated to the ectoderm induction factors; I) Mesoderm differentiated cell spheroid highlighting Brachyury expression. Inset of a single ELB that without mesodermal induction factors; J) Cell spheroids/ELB differentiated into endoderm cells detected by positive Sox17 expression; J') The SMc un-treated ELB stained for Sox17; K) Pre-programmed ELB/spheroid administered with BMP-2 to express Osterix; L) Programmed ELB/spheroid administered to BMP-2 and expressing the Runx-2 osteogenic bone marker; L') Comparative control showing a single SMc untreated ELB/spheroid treated to anti-Runx-2 fluorescence-labeled antibodies; M) Confocal laser scanning microscope (CLSM) image of an attached ELB after 7 days showing the ejection and spreading of Nanog+ cells on vitronectin coated TCP well at high efficiencies; N) A 7-day Oct3/4 positive staining of cells growing on TCP in 2D previously ejected from a 4-day old ELB/spheroid; N') Non-SMc treated cells released from the spheroid/ELB and growing as a monolayer on clear TCP and stained with anti-Oct3/4 fluorescence tagged antibody complex (note some of the subcellular localisations of the transcription factors); O) ESC108 dye positive staining of clonal cells from five individual spheroids/ELB at 7 days; P) Sox2 positive immunolabelling of clonal hmciPSCs at 14 days; Q) Plated hmciPSCs ejected from an SMc untreated spheroid/ELB at day 14 stained for SMA and showing no positive green fluorescence immunolabelling; FACS analysis of 2D plated hmciPSCs after 21 days for R) Oct3/4 and S) Sox-2 (the red peak to the left is the HDF untreated (unprogrammed) control partitioned from the same source of HDF cells (P17-27); Images shot of B to Q by a confocal laser scanning microscope (CLSM).

Interestingly, the ELB dissociated, and tissue culture plate (TCP) seeded cells from the spheroids usually developed on transparent TCP against the established convention for organic growth on vitronectin and Matrigel substrates.

Thus, the biomimetic, ELB/spheroids aggregated with 10 000 ESC-like positive cells, planted (Figure 2M) inside

6.94 mm wells, and swiftly began to dissociate and self-seed into expanding monolayers. Cell spheroids treated in this way steadfastly maintained expression of the critical hmciPSC transcription factor markers, Oct 3/4 and Sox-2 on day 7 (Figure 2N,N',O,P, and Figure S1B–D (Supporting Information)). Cell spheroids also kept on expressing the ESC-specific

2000071 (5 of 21)

ADVANCED
SCIENCE NEWS
www.advancedsciencenews.com

ADVANCED
BIOSYSTEMS
www.adv-biosys.com

marker (ESC108) for the ribosomal protein (Rps8) S8 from the small 40S unit in human cells at day 7 (see Figure 2M). In contrast to the untreated HDF's, ejected from the ELB that stained for the visible presence of vimentin (primitive mesenchyme marker = fibroblasts) at day 7, SMA at day 14 (Figure 2Q; Figures S1D and 2A, Supporting Information), and collagen I (Figure S2B, Supporting Information). Similarly, cells ejected and attached to impervious TCP surfaces failed to sufficiently express the pluripotency markers Sox-2 (Figure S2C, Supporting Information) and Oct3/4 (Figure S2D, Supporting Information). However, on the 14th day of the cell sheet cultivation the observed frequency of Oct ¾ and, direct Sox-2 expression decreased to 1% and 7%, respectively. FACS technique determined this (Figure 2R,S).

2.3. Encapsulation of Dissociated HDF Cells for Reprogramming: Parameters for Cell Densities and Distribution

Spheroids contained the transiently expressing tdTomato DNA plasmid, at very high concentrations of 10 µg mL^{-1} alginate-ECMp compared to standard plasmid concentrations added to cultured cells. The plasmid was mixed in the alginate-ECMp solution before bead fabrication. In **Figure 3**A, two independent spheroids or ELB's are exhibiting a robust red fluorescence caused by the spontaneous transfection by the naked DNA plasmid vector 48 h following coencapsulation[41] (Figure S3A, Supporting Information).

We tested the possibility for small molecule compound delivery toward completely dissociated cells and small cell aggregates (Figure 3B–Q). Encapsulation of HDF cells inside alginate-ECMp leads to heterogeneity in spatial distribution and organization of HDF cells. Approximately 25–50% of cells positively labeled for ESC108 dye (Figure 3B); whereas untreated HDF cells all failed to incorporate and express the same dye (Figure 3). Reprogramming occurred consistently in both small and large droplets up to a maximum of 523 mm³.

We also reaffirmed the ability of the small fused droplets to differentiate the already programmed HDF cells by immersing the droplets in a BMP-2 supplemented media after the fourth day of reprogramming. We detected the BMP-2 induction of newly transformed hiPSC's into Runx-2 positive cells (Figure 3C). Reprogramming appeared independent of how the cells distributed themselves after droplet formation. Cell density ranging between 1×10^5–2.5×10^6 did not affect either on reprogramming outcome (Figure 3C–F). Dissociated HDF cells inside the fused alginate-ECMp droplets randomly formed small HDF cell clusters made up of between 30 and 100 cells. We calculated programming rates averaging 64% using the ImageJ assisted manual cell counting methodology (Figure 3C–F). All alginate droplets with HDF's and the absence of a reprogramming factor expressed the fibroblast- related vimentin, collagen I and SMA antigens. The physical and chemical forces applied to the cell populations by forced encapsulation and confinement inside the droplets (Figure 3E,F).[38] Cell confinement in a rounded-up conformation facilitates the uptake of small molecules into the cell, presumably by favorably reorganizing the cytoskeleton.

2.4. Mechanical and Chemical Somatic Cell Reprogramming Inside Single Polysaccharide Droplets

The cells inside small molecule loaded alginate-ECMp's, and including GRGDS-MVG (High Guluromic acid (G) (G/Mannuromic acid (M) Ratio: ≥ 1.5) high MW)-ultrapure alginate (NOVATACH, NovaMatrix©) expressed a variety of pluripotency determinants. These include Sox-2 (Figure 3G,G'), and Nanog (Figure 3H,H'). The result against the staining for vimentin was negative in SMc treated droplets (Figure 3I,I'). The embedding of HDF cells in ultrapure alginate (High G), increased viability, growth, and stability of the HDF cells. Reprogramming occurred at high efficiencies of up to 50%. We calculated viability of 93–95% for Protanal and 97% for RGD Novatach alginate containing droplets. Decreasing cell viability over the next 7 days occurred in both types of alginates with the minimum threshold for RGD alginate being 85%. Embedding HDF cells in the pharmaceutical-grade alginate (High M), similarly led to the expression of the main pluripotency determinants: Sox-2 (Figure 3J,J'), Oct3/4 (Figure 3K,K'), dual positive SSEA-4 and Nanog (Figure 3L) and Sox2/Oct3/4 (Figure 3L'). Furthermore, ESC108 (ESC108, $C_5H_{4_6}ClN_3O_2$), the targeting molecule of the 40S ribosomal protein s8 (Rps 8), was comprehensively expressed by cells evenly throughout the entire droplet (Figure 3M,N,O). The alginate droplets swell due to osmosis and after 2 weeks burst apart. However, the bursting between individual beads is erratic. This can be corrected by oxidation of alginate.[47] The process is somewhat erratic, particularly in the lower grade of alginate. As a result of the beads bursting apart, the cells inside were released onto the culture well surface where they attached. The reprogrammed hmciPSC's released after bursting maintained their pluripotent phenotype, as they grew on the TCP surface. The confirmation of cell pluripotency was done by showing the expression of TRA-1-61 (Figure 3P) and TRA-1-81 (podocalyxin) (Figure 3Q). The ejection of cells due to bursting of beads is a useful mechanism for 2D plating and further expansion of the cell population (Figure 1A). The released cells, following the in-droplet reprogramming, maintained the pluripotency indicators shown at 7 days onward from their release.

2.5. The Structural Design of Droplet Interiors for hmciPSC Differentiation by DF Diffusion Sequential Control

In the first examination of controlled diffusivity for a nested encapsulate, we traced the complete emptying of a red histological dye from one nested 3 mm guest bead (14 mm³) into its 8 mm (268 mm³) host (seven to ten days, $n = 3$; **Figure 4**A). Bead membranes were purposefully thickened from 2–3 to 21 µm (Figure 4A,B) and stiffened by calcium phosphate deposits to reduce the diffusivity of the regular mm-sized fused droplets by reducing the nano porosity (Figure 4C,D).

The membrane is composed of polymerized chitosan electrostatically complexed on the inner side with alginate-ECMp, and a semi-crystalline calcium phosphate (Figure S4A–C, Supporting Information) coating the outer surface. Nanopores are also formed uniformly across the membrane, ranging between
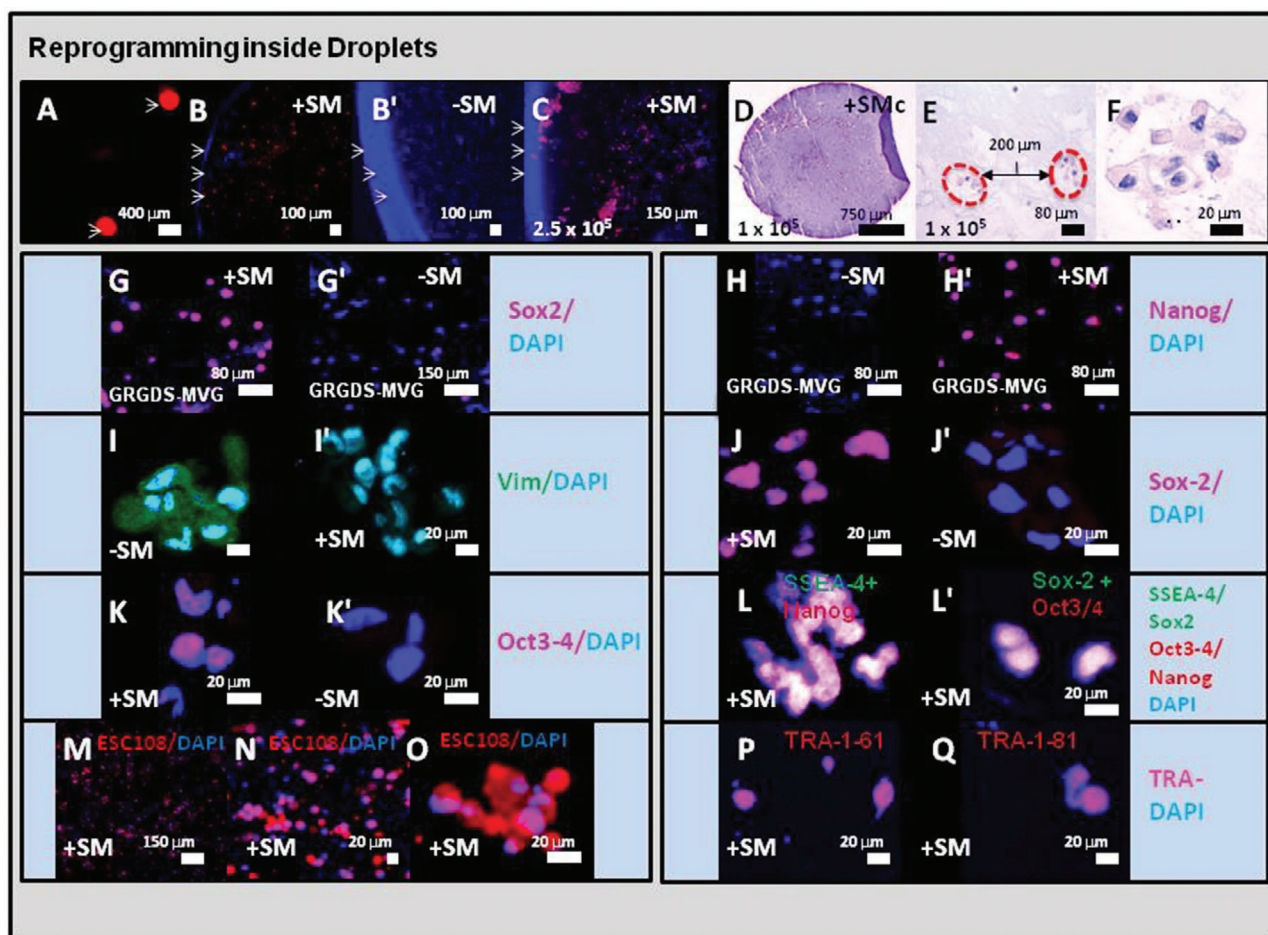
Figure 3. Encapsulation of dissociated HDFs in mm-sized fused droplets for mechanical chemical reprogramming and differentiation. A–Q) Images obtained using CLSM; A) Two encapsulated individual spheroids/embryoid-like bodies after Tomato plasmid (pCIG-tdT) transfection in the alginate-ECMp bead; B) Low power (×25 Mag) view of a large part of the droplet perimeter and part of the core containing ESC108 positive cells following 4-day reprogramming; B') The comparative image of a no-SMc droplet containing unprogrammed cells; C) Low magnification (× 25Mag) image of a droplet containing ESC 108 positive dissociated cells and cell clusters following SMc reprogramming in 3D; D) Combined hematoxylin and eosin (H & E) staining of a single cell-laden droplet to show the distribution of dissociated HDF cells; E) H & E stained section through a droplet containing HDF cells to show the tendency for the clustering of which some may be clonal colonies, generated while growing in the alginate droplet; F) High magnification (×1000 Mag) image of a small cluster of programmed pluripotent cells; G) Partial in situ view of a single SMc (the RPF), treated GRGDS-MVG (High M; High MW) alginate droplet, at day 7, labelled for Sox-2 compared to a similar droplet without SMc G') with the absence of positive Sox-2 immunofluorescence. H) In situ cell staining for Nanog (purple) between the SMc untreated GRGDSP-MVG droplet, and H') the treated droplet. I) An individual HDF 3D cell cluster labeled for vimentin (Vim – green) following 7-day encapsulation in an alginate-ECMp droplet; I') An individual HDF cell cluster treated to ProgramimTM (mciPSC) in alginate-ECMp labeled for vimentin; J) SMc programmed cells highlighted by pluripotency related Sox-2 (purple) labeling J') and unhighlighted among unprogrammed cells. K) Oct3/4 positive cells programmed by SMc's in alginate- ECMp fused droplets and K') unprogrammed cells inside ECMp droplets; L) SSEA-4/Nanog-positive cells programmed by alginate-ECMp fluorescently labeled on thin sections; L') Combined Sox-2 and Oct3/4 labeled cells in Programin (mciPSC) alginate-ECMp. ESC108 stained human cells, imaged in situ, programmed by alginate-ECMp after 4 days at different magnification, starting at a M) low × 100, N) × 200 and O) high magnification of × 500; M,N,O images are taken from the same group of droplets; Labeling for P) TRA-1-61 andTRA-1-81; Q) by cells released automatically from mm-sized fused droplets onto the TCP surface on the first day from the ELB or spheroid release (n = 12). Note that light blurring in some of the images occurred because the image was of whole 3D beads in situ. The white arrows in (A–D) refer to the edge of the host droplet, expansion (Figure 1A). The released cells, following the in-droplet reprogramming, maintained the pluripotency indicators shown at 7 days onward from their release.

250 and 300 nm (Figure S4A–C, Supporting Information). However, in the 60 min formed membrane (Figure 4Bi–iii) at 50×10^{-3} M calcium concentration and used to produce the guest mm-sized fused droplets, the membrane was densely mineralized with 150 nm pores (Figure S4C, Supporting Information).

Advanced control over the membrane nanoarchitecture is possible by adjusting the degree of chitosan deacetylation, its pH, and the calcium concentration for the degree of calcium phosphate precipitation and densification (Figure 4Bi). The calcium cross-linking concentration of 5×10^{-3} M produced a thin membrane and large porosity, which would lead to more
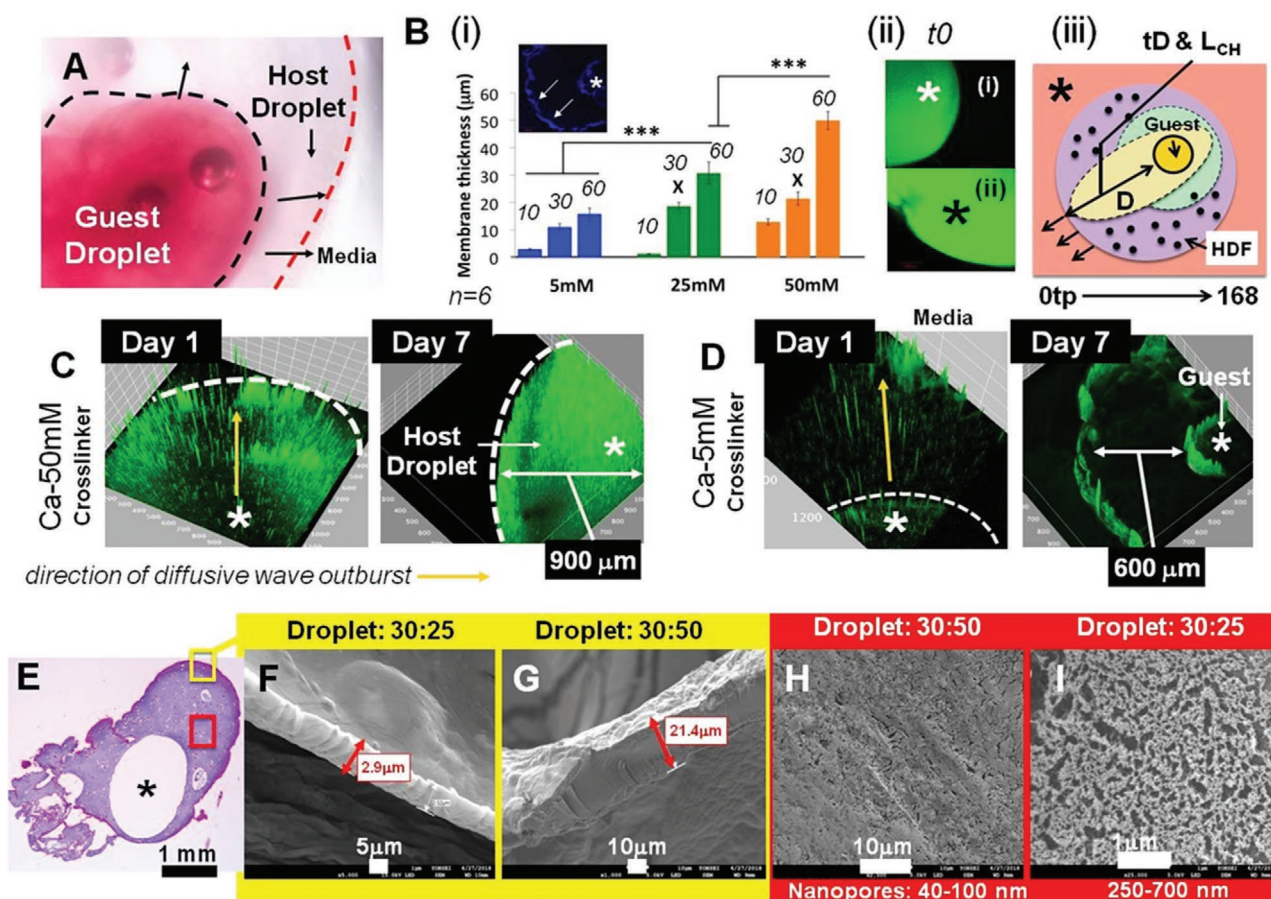
Figure 4. Nested droplet time-controlled diffusion and cell differentiation. A) Microscopic brightfield light image of the nested arrangement of a single guest bead captured in situ. The guest bead is stained with alizarin red while the host is undyed. The perimeter edge of the host bead is marked dotted red. The dashed black line outlines the perimeter of the guest droplets, and the black arrows refer to the probable direction encapsulate diffusion; Bi) A graph of membrane thicknesses between different levels of calcium in the chitosan solution and over increasing periods (10, 30, 60 min) for the membrane-forming reaction. The X's in ii) denote the time (10, 30, 60 min) for the membrane-forming reaction. The X's in (ii) denote the individual droplet with fluorescent particles and the external media in (iii), respectively. The inset is a confocal image of membranes in blue fluorescence. Arrows point along the direction of diffusion, and the star denotes the origin of the fluorescent particle concentrations). ii) Green fluorescent Dextran loaded bead; a) 20 kDa and b) 70 kDa at time origin (t0). iii) The graphical conception of the bead-in-bead DF controlled release system also showing the parameters used to describe the behavior of the hydrogel, such as diffusivity, elasticity, stiffness, and hydrogel flow and relaxation[46] 0tp to 168 refers to the time in minutes from origin to 168 min. The arrow inside the dark yellow region denotes the parameter LCH. D = Diffusion, tD = diffusion time, LCH = Length of diffusion. The arrows are pointing outward from the purple region highlight (the direction of diffusion from high concentration to low concentration of the concentrated dextran solute). 10 kDa Dextran particles fluorescently traced and broadly showing the distribution in C) low calcium concentration mm-sized fused droplets (5×10^{-3} M), and D) high calcium concentration mm-sized fused droplets (50×10^{-3} M), between 1 and 7 days (white star = Alginate-ECMp, yellow arrow = direction of dextran diffusion). The particles match the size of DFs used for germ layer cell transformation typified by BMP-4, Activin A, and wnt3 (Table S1, Supporting Information). E) A complete thin section across a single mm-sized fused droplet of alginate. F,G) The yellow square shows a region imaged via a Scanning Electron Microscope (SEM) revealing the chitosan/CaP membrane. The red square highlights the position corresponding to the SEM images in parts (H) & (I), revealing the alginate core nanopores. F) Bead membrane formed by a 30:25 Ca:P ratio, and G) by a 30:50 Ca:P ratio. H) Alginate and ECMp core, made from the 30:50 chemistry parameters, to show the 40–100 nm nanopores. Note that the cytoplasm of some of the cells has also incorporated the DAPI cell nucleus stained leading to nonspecific autofluorescence in the image panels. The stars (*) in parts B(ii), (iii), (C), (D) and (E) denote the place of the nested droplet.

rapid diffusion rates (Figure 4C). A sharp increase in the calcium ion supplementation of chitosan from 5×10^{-3} to 50×10^{-3} M (the upper limit for cell toxicity from previous studies with the polysaccharide droplet or beads or capsules[30] thickened the membrane along with longer chitosan immersion times spanning 30–60 min. Membranes varied in thickness among 5, 11, and 17 µm by 5×10^{-3} M of calcium ions, 2,

19, and 30 µm with 25×10^{-3} M, and 13, 21, and 42 µm with 50×10^{-3} M of calcium at 10, 30, and 60 min immersion times in the calcium supplemented chitosan counteracting solution (Figure 4Bi). Calcium ion cross-linking of alginate-ECMp influenced the matrix nanopore size, confined by the degree of M units in the polymer (M/G 65:35 and M_W between 250 and 350 kDa), and high, 50×10^{-3} M calcium

**ADVANCED
SCIENCE NEWS**
www.advancedsciencenews.com

**ADVANCED
BIOSYSTEMS**
www.adv-biosys.com

concentrations reduced pores to 4–20 nm (Figure 4H; Figure S4A, C, Supporting Information). Alginate-ECMp nanopores controlled passive diffusion into the media, which was also restrained by the membrane and the level of porosity tested in experiments between droplets with different chemistry parameters, based on calcium ion concentration and chemical I). We did not attempt to vary the molecular weight singularly, the M/G ratios, which determine the crosslinking density and distribution, together with determined lengths of the G and M blocks.[48] These characteristics configure highly specific physical, mechanical, and cell compatibilities and responses. Dextran-FITC particles with an identical size to the DF's, ranging between 10 and 70 kDa simulated the following assorted DFs investigations into their diffusive properties (Table S1, Supporting Information) between time origin (Figure 4Bi,ii) and at day 7 (Figure 4C,D) for the 10 kDa particles. High-resolution (at × 1000) CLSM imaging traced the emptying of the guest and host mm-sized fused droplets by Fluorescein isothiocyanate (FITC)-dextran. The even spreading and containment of dextran particles in the 50×10^{-3} M, mm-sized fused droplets (Figure 4D, day 7) was in contrast to the 5×10^{-3} M (Figure 4C) and 25×10^{-3} M (Figure 4F,I) mm-sized fused droplets. Here the Dextran particles were tightly confined to the membrane (Figure 4C), and the majority of dextran had diffused into the exterior environment by comparing and contrasting status at Figure 4Bi,ii showing the fluorescence of the guest droplet with Figure 4C,D showing the fluorescence in the host droplet at day 1 and day 7 (Figure 4C,D). This was further confirmed by the strong fluorescence signal in the exterior media containing the droplets. Within 24 h the fluorescent dextran particles diffused against the internal edge of the host droplet. However, it takes up to 7 days for the dye to reach peak concentration inside the host droplet. In contrast, dextran particles diffused very rapidly, with 85% of the dextran content emptied from both mm-sized fused droplets, leaving approximately 15% of the dextran remaining in the host. These estimates were based on calculations of the surface area occupied by green fluorescence, in 2D planar snapshots. We shall model the diffusion pattern within mm-sized fused droplets mathematically and pictorially. In evidence that the DF successfully diffused from the nested droplet into the host droplet, the staining for differentiation occurred within a 500 μm visible corona (Figure S7B,D, Supporting Information) since we did not label it for observation, and provided functionality to the subsumed cells.

In this set of experiments the mesh size, cross-linking density and molecular weight parameters were not adjusted for the tenability and optimisation of the process of diffusivity for the molecules in the solvent, as well as the mechanical properties. The mathematical model using the parameter inputs for the correct alginate describe its behavior accurately as

$$T_{\rm P} > t_{\rm R}, \text{ and } T_{\rm P} > t_{\rm D} \tag{1}$$

where $T_{\rm P}$ = process time (24–168 and 240 h) and $t_{\rm R}$ = viscous relaxation time (8 h where $t_{\rm D}$ = diffusion time (0.081 h)).

Equation (1) describes the alginate used as "an elastic solid with relaxed moduli and pronounced migration of solvent"[46] (Figure 4Biii).

The process conditions are more dynamic, because of the long-range movement of the solvent so that the alginate behaves as both a viscoelastic and poroelastic ($t_{\rm R} < t_{\rm D}$) solid used to simulate the diffusive behavior of the hydrogel.[46] Therefore, not only can we control the diffusion of the DF's by the interposition of semi-permeable membranes and micro-/nano porosity, but also by the molecular weight of the polymer between the cross-links (Mc), but only in a minimal way. Future use of this model shall provide the specific set of design criteria for alginate droplet biomaterials with specified mechanical behavior that is relevant to influencing cell function and behavior.

2.6. Mechanical and Degradation Properties of Droplets

Physical and mechanical properties of the droplets define the robustness, the chronology and pattern of escape and clearance of the cell conversion proteins, the stability of the system, the level of physical support to embedded cells, and the strength to withstand in vitro manipulation and transplantation. Mechanically two parameters are essential to evaluate the functionality to carry out several design purposes; the shear modulus and Young's modulus. Hydrogels are notoriously weak, soggy, and soft materials. In our droplet system, the intermingling of chitosan and alginate reinforces the structure increasing its resilience to compression. The membrane adds robustness again in compression and reduces swelling. Four parameters about the polymer (**Table 2**) were used to identify and calculate the basic mechanical properties of the droplets in the equilibrium state. Alginate-chitosan droplet stiffness (E) approximated to 150 kPa in compression in pH neutral media, while 20 kPa for tensile strength.

Degradation occurs first by fragmentation at 7 days (+/−2) for bare alginate as the burst and fracture, and from 14 days in chitosan-coated alginate-chitosan droplets. Nested droplets follow a similar pattern after release from the host droplet.

2.7. Quantitative Analysis of Diffusion Inside Droplets

The characteristics of passive diffusion through hydrogels set-up the relative concentrations of encapsulated proteins and distributions over time. The accurately timed suspension

Table 2. Molecular parameters for alginate and chitosan biopolymers essential to calculating their mechanical properties.

Parameters	Alginate hydrated & linked	Chitosan hydrated & linked
Mesh Size	5 nm	50 nm
Block Residue Mol. Wt. (M_r)	193.13 g mol^{-1} [M-rich]	179.17 g mol^{-1} [DA 95%]
Mol. Wt. crosslinks (M_c)	386.26 g mol^{-1}	663 g mol^{-1}
Length of bond (l)	0.9 nm	1 nm
Diffusion coefficient D (cm^2 s^{-1})·10^7	1–2	3.4–6.1

2000071 (9 of 21)

of functional concentrations of proteins is essential for proper cell activation for reprogramming and differentiation. The small protein molecules, DF's, reprogramming factors, and ECM components were physically trapped, confined, attracted, and bound to the polymer as well as suspended and confined between the polymer strands. We hypothesised on the associations of the ECM proteins and conversion factors with the polymers, which impacts on diffusivity (Table 2). Experimental and mathematical approximations measured the diffusivity of water through the droplets.[42–44]

The diffusion rate was related to the degree of 3D swelling of the alginate polymers to the equilibrium configuration. The diffusion coefficient also determines it for alginate and chitosan ($(D$ (cm^2 s^{-1}) $\times 10^7$)[45] and a molecular weight between the crosslinks. The quantitative data for swelling and diffusion fluxes of water containing these small proteins (the physical and chemical properties listed in Figure S6 in the Supporting Information) described and explained the movement across the three structurally defined concentric regions of the droplet; alginate, alginate chitosan interpenetrating network (forming the acid gel region) bounded by the semi-permeable chitosan membrane. (Figure S7, Supporting Information). The key indicators are swelling capacity, and the diffusion coefficient, which can be calculated using prescriptive equations[46] and accurately by tracing dye-tagged molecular diffusion of 39 kDa (equaling the median mol. Wt. of DF proteins) egg yolk phosvitin (fluorescently tagged phosvitin Antibody (D-5): sc-46681) protein molecules in an apparatus containing the chitosan/calcium phosphate coated alginate core. Diffusion coefficients for the chitosan-calcium phosphate coated alginate tubes began with 1.8×10^5 cm^2 s^{-1} in the first five hours and 1.2×10^5 cm^2 s^{-1} after that for 7 days, compared with higher values in bare alginate cylinders of 3.2×10^5 cm^2 s^{-1} (Table 2; Figure S8, Supporting Information). So, within 15 h, the leading edge of the diffusion front meets the outer membrane trapped and filtered. Behind the leading edge remains a relatively uniform concentration of the diffusing proteins. From the previous tracing results, the molecules become trapped at the membrane delaying the outer release. Previous coefficients for proteins 25 and 63 kDa were calculated at 2.1×10^6 cm^2 s^{-1} (a-chymotrypsin) and 1.6×10^6 cm^2 s^{-1} (serum albumin) respectively.[43] Some visible swelling occurred in the alginate-chitosan droplets in the first two hours of immersion and stabilized ($V = 8.18$–22 mm^3). However, swelling occurred in chitosan-coated droplets reinforced with calcium phosphate precipitate. Thus, it appeared the reinforced membrane acted as a counterforce to the small-scale swelling ($V = 8.18$–14.4 mm^3) of the alginate core due to the chemical balancing of salts and chemical gradients between the alginate and external water phases (Figure S7, Supporting Information). Mobility and the inevitable release from the droplets are controlled by diffusion mechanics and not swelling with solvent exchanges.

2.7.1. Time and Space Evolution of Cell Conversion Signals

To fine-tune the control of conversion signals for differentiation and reprogramming its essential to model the binding and diffusion characteristics in the hydrogels related to their structure,

architecture, chemical properties, and mechanical properties. Multivariate modelling of diffusible factors inside hydrogels is intricate. So far, we have worked with a trial and error optimization approach to converting cells in predetermined lineages. These results are phenomenological. We were able to describe diffusion behavior, mechanical behavior, and swelling by solving a range of differential equations from four parametric inputs about the polymer.[46]

Our concept is to think of the proteins concentrated in the nested droplets and releasing unbound and unconfined small proteins in a concentric ripple into the host droplet, as depicted in Figure S9 in the Supporting Information. The outer droplet space covers itself at a moderate rate in the alginate gel and a lower rate in chitosan hydrogel. Our experimental and use of models tracked DF solutes ranging in sizes between 300 Da and 60 kDa/1–3 nm. The small reprogramming molecules were mixed droplet wide. Their diffusion was limited by the chitosan-alginate gel domain and the semi-permeable chitosan-calcium phosphate membrane principally through binding to the positive charges on the chitosan polymer. Models that predict solute movement characteristics through alginate hydrogels by integrating hydrodynamic, free volume and obstruction theories are reasonably accurate at determining mass transport phenomena for a range of solute sizes, including the size range of DFs.[49]

2.8. Calculated Reprogramming and Differentiation Efficiencies Inside Programin (mciPSC) mm-Sized Fused Droplets and Nested mm-Sized Fused Droplets

The spheroids/ELB's, when plated, seeded the viable hiPSC's onto the TCP surface and clones formed for 14 days, generating a continuous monolayer. Another FACS calculation, however, showed that by 21 days, the pluripotency markers expressed themselves at levels of 1% for Oct3/4 and 7% for Sox2. High levels (>1%) of reprogramming occurred inside mm-sized fused droplets containing the reprogramming factors. The high reprogramming rates are shown graphically in **Figure 5**A–C.

The same nested mm-sized fused droplets without the DF containing guests displayed no positive staining for the germ layer cell identities (Figure S6B–D, Supporting Information**)**. In the droplet manipulation trials for endodermal differentiation, two nested mm-sized fused droplets delivered one burst of Activin A, FGF, and wnt3, followed by another discharge of Activin A and FGF (Table S1, Supporting Information; Experimental Section) from the second more heavily mineralized guest bead (50×10^{-3} м cross-linked for 60 min). The nested guests contained the standard nanogram cocktails of DF's for 3-germ layer cells, permeating the dissociated hmciPSCs which were reprogrammed at 21% programming efficiency at day 3, and 24.5% (+/−2%) at day 5 by FACS analysis for Nanog+ cells (Figure 5A,C) throughout the host droplet. The increased population of positively reprogrammed cells is a good indication of the diffusion mechanics inside the droplet. Existing among the original population of HDF's, those partitioned inside droplets containing BMP-2 guests were reprogrammed and differentiated. Converted Runx-2 positive cells totaled, on
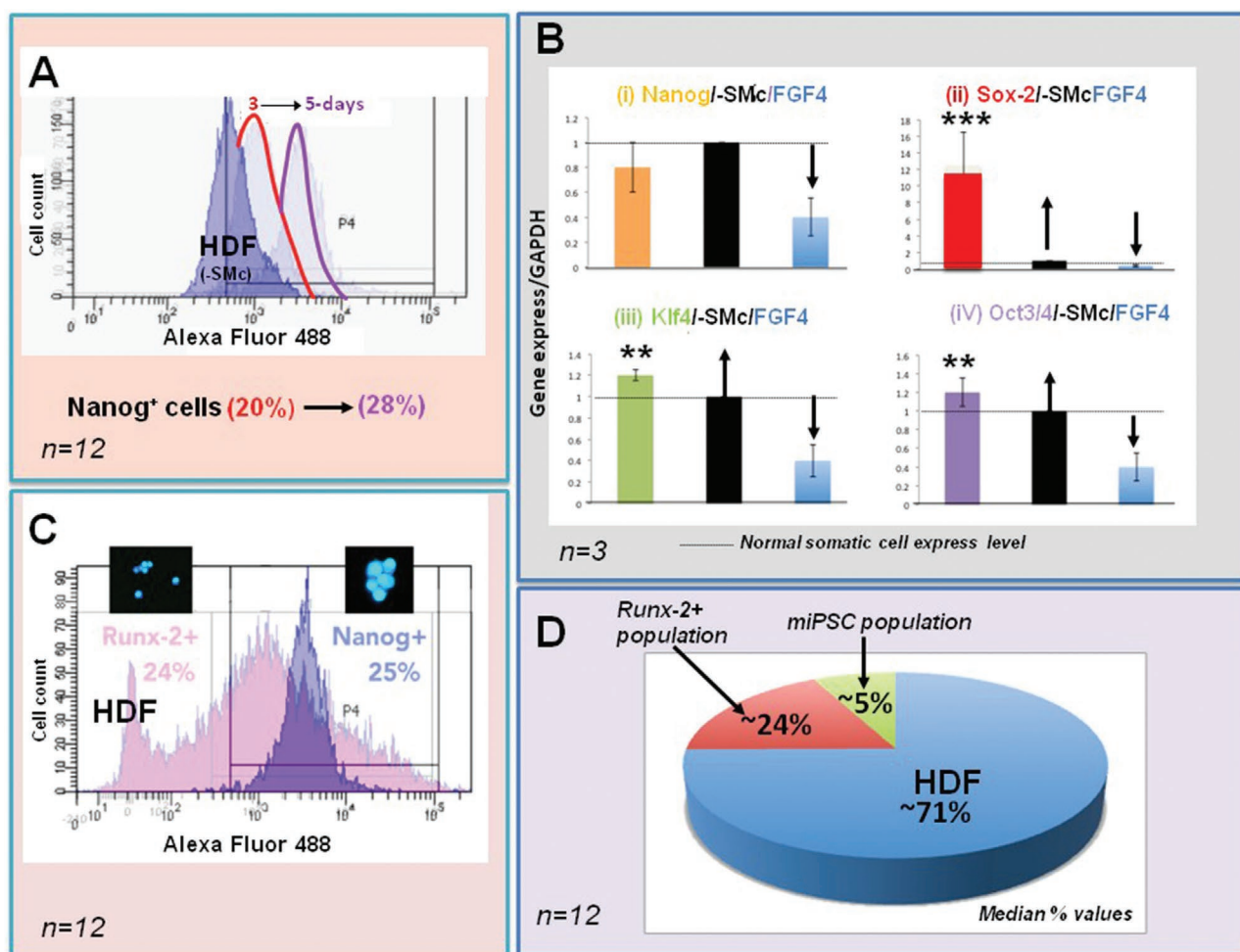
Figure 5. Numerical analyses of cell identities inside single and multidroplets (one guest). A) FACS analysis re-runs showing the proportion of Nanog+ positive cells released from Programin (mciPSC) mm-sized fused droplets at 3 (20%) and 5 days (28%); B) RT-qPCR measurements of gene up regulation for the pluripotency defining transcription factors: i) Nanog (yellow bar), ii) Sox-2 (red bar), iii) Klf4 (green bar); iv) Oct3/4 (purple bar), and the downregulation of HDF specific FGF4 (Black the bar is the RQ level for untreated HDFs; the blue bar is the FGF4 down-regulated level). The gene expression level was normalized to the GAPDH housekeeping gene on the y-axis. The horizontal line is for normal expression levels of pluripotency genes). Furthermore, the data ran in triplicate from 3 separate samples; C) HmciPSC's in alginate-ECMp after programming express Nanog+ by FACS analysis at day 5 in the blue peak and following BMP-2 diffusion from the guest the expression of osteogenic Runx-2 at day 7 in the pink peak. The second peak to the left represents the HDF population. The inset panels in C shows the CLSM image of positively labelled cells used in FACS analysis. D) A graph displaying the manual cell counts of positively reprogrammed cells, differentiated cells and HDF cells inside typical droplets, represented as a percentage % of the total cells loaded into the original droplets (the percentages are rounded-down for clarity, and the n = represents the number of separate experimental samples derived from 15 large droplets, and each FACS run was done in triplicate).

average, 25% of the single-cell population. This also means a 99% interconversion between Nanog+ cells and osteogenic derivatives (Figure 5C). In the absence of SMC, not only is there no expression of pluripotency genes, but there is also no expression of osteogenic markers with BMP-2 present in the droplet environment. It is, therefore, not biologically possible to convert HDF cells into osteogenic variants by BMP-2 treatments alone. Figure 5B shows the reprogrammed HDF cells inside alginate droplets expressed the pluripotency defining (i) Nanog (yellow bar), (ii) Sox-2 (the red bar), (iii) Klf4 (the green bar) and (iv) Oct3/4 (the purple bar) genes for the transcription factors at fold changes significantly higher than the untreated HDF cells in SMC-free alginate droplets (the black bar). The

measurements came from quantitative reverse transcription-polymerase chain reaction (RT-qPCR). The healthy gene representing HDF cells, FGF-4, was suppressed or downregulated by SMC treatment, as shown by the height differences between it (blue bar) and the black bar (representing the expression levels among untreated HDF cells). A problem for the system is the heterogeneity of cell identities in terms of the genome expression landscape following SMC reprogramming and the onward differentiation using the nested droplet mechanics (Figure 5D). Following the maximum reprogramming and differentiation using singularly precise concentrations, there were approximately 71% of HDF cells, 24% of Runx2 positive cells, and a 5% population of programmed hmciPSC's (Figure 5D).
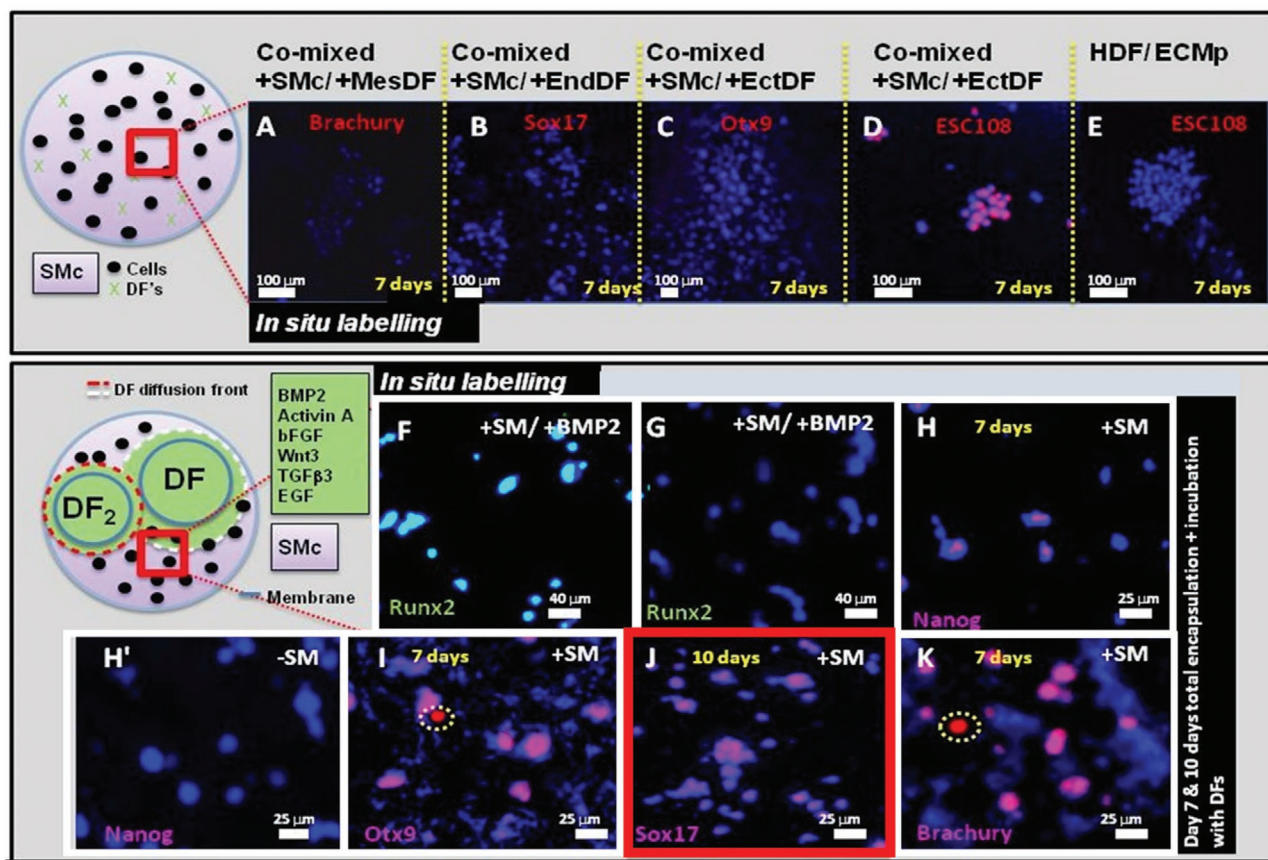
Figure 6. In situ fluorescence tagging of cell identities to demonstrate the sequenced in vitro (static culture) HDF cell reprogramming and differentiation into osteogenic cells and germ layer cells by the nesting of DF mm-sized fused droplets. A–E) Results from the alginate-ECMp mm-sized fused droplets containing a co mixture of RPF and DF's for germ layer cell formation (Activin A, FGF, wnt3). Alginate-ECMp mm-sized fused droplets containing a comix of Programin (mciPSC) and DFs in (A) for mesoderm (+SMc/+MesDF) showing minimal expression of Otx2, in B) for endoderm (+SMc/+EndDF) and C,D) for ectoderm (+SMc/+EctDF), repeatedly showing minimal expression of C) Otx2, A) Brachyury, and B) Sox7 after 7 days of static culture. Therefore, in comixture droplets, the cells were reprogrammed, but not simultaneously differentiated. D) Results of reprogramming in comixed fused droplets showing positive ESC-like cell labelling. E) The cells inside droplets without RPF and DF's showed no expression for any marker of PSC or differentiation. F) Runx2 positive 7-day cultured cells in an SMC and BMP-2 co infused droplet at low power, and G) at high power. This, in contrast to droplets without RPF content, but containing BMP-2 and stained for Runx-2. H) Nanog+ positive cells populating an alginate-ECMp droplet containing SMc and a single nested BMP-2 droplet at day 4. H') Embedded 7-day cultured cells untreated to SMc that stained with anti-Nanog. I) Embedded hmciPSCs in alginate-ECMp and presented with the DF's for ectoderm induction expressed Otx9 (Pink is representing costaining of antigen plus DAPI nuclear stain, dotted circle = unfocalized fluorescence artifact). J) Embedded hmciPSCs in alginate-ECMp and twice exposed to DF for endodermal cell induction from 2 nested droplets with individual membrane thicknesses and permeabilities -positively expressing Sox17. The red border surrounds the small area of a droplet with Sox17 positive cells at day 10. K) Embedded hmciPSCs in alginate-ECMp and exposed to DF for mesoderm induction positively expressing Brachyury (dotted circle = unfocalized fluorescence artefact. The extra blue patches are the result of alginate impurity, and calcium phosphate derived autofluorescence).

2.9. United Cell Reprogramming and Differentiation within In Vitro Cultured mm-Sized Fused Droplets

Using the nested droplet arrangement, we were able to sequence reprogramming and differentiation (**Figure 6**A–K). It makes sense to deliver multiple growth agents and morphogens in a deterministic sequence rather than in combination inside the droplet (>1). Single BMP-2 mm-sized fused droplets nestled into SMC mm-sized fused droplets led to the emergence of Runx-2 positive cells within 7 days, including the initial 4-day reprogramming period (Figure 6F, G). Efficiencies varying between 21% and 34% occurred, measured by ImageJ, which assisted counting to increase accuracy and reliability. The numbers of positive cells mirrored the numbers of Nanog+

cells determined by immunofluorescence, even accounting for the potential of autofluorescence (Figure 6H,H'). Once again, zero-SMc fused droplets were Runx2 and Nanog- negative following antibody labeling. Therefore, we can reasonably assume that the positive osteogenic cells had derived from the iPSC population. The mm-sized fused droplets with the three germ layer DF's led to hmciPSC downstream conversion into these progenitors, at the rate of 23%, 46%, and 79% for Otx2 (Figure 6I), Sox17 (Figure 6J), and Brachyury (Figure 6K) genotypes, respectively. Sox17 cell expression was measured at 10 days, including the 4-day reprogramming, requiring two nested guest droplets to deliver one cocktail of 3-individual DF's, which followed after 2 days with the second delivery of a similar cocktail of DFs; according to the previous results for germ

**ADVANCED
SCIENCE NEWS**

www.advancedsciencenews.com

**ADVANCED
BIOSYSTEMS**

www.adv-biosys.com

layer cell induction (the StemPro© differentiation kit) (Figure 1Aii; Table S1, Supporting Information). Further sequencing involved a second delivery of the DF cocktail through a droplet having a thicker membrane (21–25 mm (Figure 4G) to delay the diffusion sufficiently at day 6 (4 reprogramming days + 2 days DF exposure). The Otx2 and Brachyury conversions mismatch the percentage of cells converted by SMC alone by an extra 23% and 56%, respectively. The germ layer cell DF's concentrated at functional levels (although not necessarily corresponding with the initial concentration inside the guest droplet) by diffusion from the guest droplet on days 6 and 7, markedly inside a 500 µm zone around the guest membrane (Figure 4C,D; Figure S6A–D, Supporting Information).

### 2.9.1. United Cell Reprogramming and Differentiation within Implanted mm-Sized Fused Droplets

Subcutaneous Pocket Transplantation: mm-sized fused droplets in the nested arrangement successfully automated the two-step process of HDF reprogramming and then reconversion into the three-germ layer cells, as in the ICM following the in vitro culture experiments. The subcutaneous pocket is the first test for experimental tissue engineering (**Figure 7**A). The mm-sized fused droplets nested with nanogram quantities of mesodermal (BMP7 and Transforming Growth Factor (TGF-β3)), ectodermal (Retinoic acid, Epidermal Growth Factor (EGF), Bone Morphogenic Protein (BMP-4), and primary (b) basic-Fibroblast Growth Factor (FGF)), endodermal (wnt3, Activin A, FGF coupled with a re-energizing of the cells with Activin A and FGF) (Figures 1Aii and 1B4, Table S1, Supporting Information; Experimental Section), and mesodermal DF mm-sized fused droplets (Activin-A and TGFβ1) were implanted subcutaneously and examined after two weeks, together with the surrounding host tissues for signs of cell dispersal, regeneration, integration, and assimilation (Figure 7A (for ectoderm as an example) and Figure 7B,B',C,D).[50] Histological staining provided evidence of hmciPSC induced carcinoma (Figure 7B), and Nanog positive PSC populations *de novo* expansion and localized dispersal (Figure 7C,D). Human leukocyte antigen (HLA)+ cells are labelled in the resident droplet zones (white stars, *) and lining the implantation sites occupied by the droplets where they permeate the host dermal tissues (Figure 7B,B'; Figure S9, Supporting Information). Basic histostaining also highlighted partially organised ectopic endodermal tissue with correct anatomical polygonal architecture (Figure 7F; Figure S7H, Supporting Information), plus small disordered assemblies of Sox17 endodermal positive cell aggregations (Figure 7E,E',E''), Brachyury positive mesodermal cells (Figure 7G,G'), and Otx2 positive ectodermal cells (Figure 7H,H',H''). Together, these suggest that the two-fold guest DF delivery is more efficacious in vivo, because it produced a germ cell specific anatomical structure unlike the mesoderm and ectoderm droplets (Figure 7F vs Figure 7E,E',E'',H,H',H''). Also, since the double mixture droplets do not produce differentiated germ layer cells, the delay in DF delivery is necessary for germ layer cell formation and the partial anatomical structures arising from them over 2 weeks. We can assume that the droplet nesting in vivo gives rise to the germ layer cells.

2.9.2. Droplet-Based Unification of HDF Cell Reprogramming and Differentiation Inside a Nonunion Bone Defect

In the advancing sequence of droplet experiments, in nude mice, we witnessed a stepwise cell reprogramming and differentiation in the nested mm-sized fused droplets following 4-weeks of implantation within a calvaria nonunion bone defect. HDF droplets however (**Figure 8**A,A'), did not promote endogenous bone reformation (Figure 8). We also observed the basic construction elements of nascent bone. The alginate-ECMp-chitosan and semi-crystalline calcium phosphate coated mm-sized fused droplets, containing HDF cells (90 000 per 2.5 mm diameter capsule) and in one of the test groups, 0.5 mm diameter guest BMP-2 mm-sized fused droplets, bridged the entire 5 mm nonunion calvaria defect (in the parietal bone of 5 individual mice with 2 droplets per defect) (Figure 8A–D). At the same time HDF cell mm-sized fused droplets were implanted into a nonunion cranial defect. We also applied mm-sized fused droplets with HDF cells but free of SMc (Figure 8A,A'), with both HDF cells and SMc's (Figure 8B,B'), and mm-sized fused droplets with a mixture of SMc and BMP-2 (Figure 8C,C') to clarify the contributing elements to bone generation. After four weeks in situ, the droplet-defect complex was detailed by immunohistology for osteogenic markers at different phases of maturity. These were Osterix (OSX or Sp7, synthesized at the early-phase of bone formation, Figure 8E), Osteocalcin (OCN, Late) and Osteopontin (OPN, Late phase, Figure 8F). A string of osteoid pearls, sandwiched between laminated fibrous collagen tissues, which may be partly derived from alginate embedded unprogrammed HDF's, indicated by HLA+ staining of this tissue, bridged the cranial defect with BMP-2 mm-sized fused droplets (Figure 8E–H). The guest capsules can be clearly identified in the yellow outline, pictured in Figure 8D. Comparing the different effects on the behavior of cells and tissues by the various droplet micro environments we observed a trend of increasing level of bone formation determined by the existence of Osterix protein, OCN, and OPN staining of tissues within the open shell of the droplets, following sectioning, and externally localized around the droplets. Significantly the comix droplets permeated into irregular, discontinuous areas of OCN and OPN expressing tissues. Anatomically correct, mineralized bone segments emerged inside the droplets containing the BMP-2 guest only (Figure 8D,D'). However, the blended droplets generated some bone-like nodules. In alginate-ECMp mm-sized fused droplets, only nonhuman derived fibrous tissue crossed the calvaria bone gap. We also observed the ignition of bone formation, elements of the early phases of modelling in the SMc carrier droplets (red dotted line), and in the comix droplets (Figure 8C,C').

Emerging osteoid and mineralized bone tissue formation at the gel droplet implant site also correlates to the *de novo* tissue type found inside SMC only mm sized fused droplets (Figure 8B,B'), SMc+BMP2, mixed droplets (Figure 8C,C') and nested BMP2 mm sized fused droplets (Figure 8D,D'; Figure S7E–G, Supporting Information). A minimal number of cells generated bone segments *de novo*. We calculated that the implantation of 180 000 HDF cells at the reprogramming rates measured in vitro would give rise to ≈45 000 hmciPSC's and the possible conversion into ≈45 000 osteogenic-potential cells. There were also other areas of mineralized bone segments.

ADVANCED
SCIENCE NEWS
www.advancedsciencenews.com

ADVANCED
BIOSYSTEMS
www.adv-biosys.com
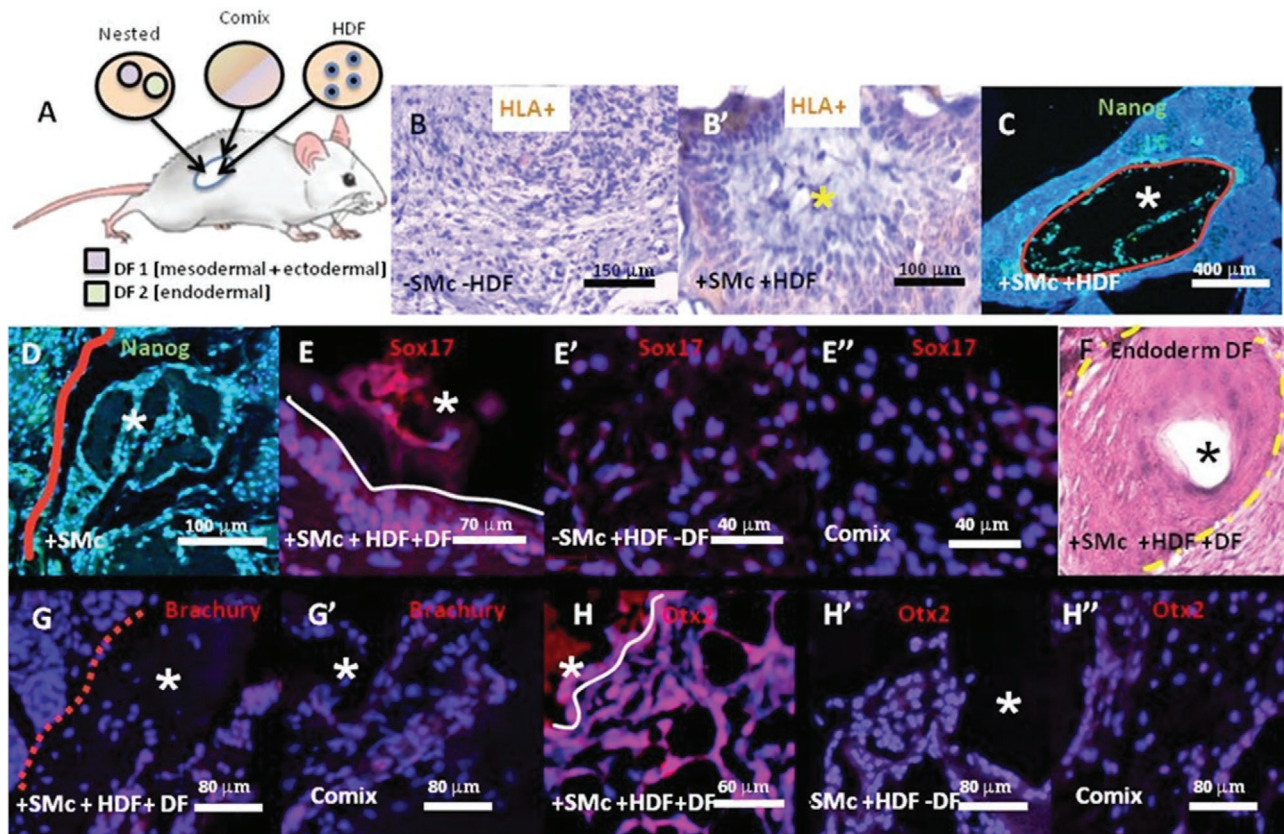
Figure 7. Encapsulated HDF's: Reprogramming and germ layer cell differentiation within an in vivo subcutaneous pocket. In vivo HDF small chemical molecule led reprogramming and growth factor conversion into the three germ layer cells after 3D encapsulation inside single and double nested SMc mm-sized fused droplets and implantation in a subcutaneous pocket of nude mice for 14 days. A) Drawing illustrating the placement of alginate droplets in a subcutaneous pocket at the rear flank of the mouse. DF nested, comix and HDF only droplets were implanted; B) HLA-1 marker unexpressed at the site of a droplet that did not contain imported HDF cells; B') Small number of HLA-1 positive cells suspended inside an implanted alginate-ECMp droplet; C) RPF droplets produced a sebaceous gland sarcoma tissue around the 2-week resorbed droplets here stained for DAPI and Nanog to illustrate successful reprogramming in vivo (C, D red line = interface between alginate and host). D) Nanog fluorescence from Programin (mciPSC) mm-sized fused droplets after 2-weeks in a subcutaneous environment at low magnification (×100 Mag). E) The emergent tissue from endoderm differentiation mm-sized fused alginate droplets recognized by positive Sox17 labelling (white line = interface between alginate and host); E') The contrast droplet without SMc (RPF) and stained for a definitive Sox17. E'') A droplet containing the commixture of RPF and DFs labelled for the presence of Sox17; F) Histoanatomical emergent cuboidal cell structure from an endoderm-inductive double guest fused alginate-ECMp droplet (yellow dotted line = interface between alginate and host); G) Brachyury positive mesodermal cells ejected from the implanted droplet that are dispersed disorderly (red dotted line = interface between the droplet and the host tissue); G') Mixed droplet labelled for Brachyury. H) Dispersed ectodermal Otx2-positive cells from a subcutaneous ectoderm droplet compared with an implanted vivo without RPF (white line = interface between alginate and host); H') Contrast droplet without MSc and stained for the definitive ectoderm marker, Otx2; H'') A mixture droplet labelled for Otx2. The yellow star (in B'), white star (in C, D, E, G, G', H, H') and black star (in F) denotes the position of the alginate droplet. The alginate hydrogel droplets were implanted into two individual mice; $n = 4$ per treatment group as illustrated in Figure 1B1–4.

Identical texture and structure to the untouched cranial bone as observed under polarized light. These segments originated from the alginate/ECMp (Figure 8D (left)), as well as the positive remodelling of the defect edge by Nanog+ pluripotent cells, and sporadically along the "sandwiched" bone regenerating tissue layer suspended across the defect (Figure S8A–P, Supporting Information). Nanog+ cells dispersed themselves in and around the SMC treated droplets, but absent from the HDF containing droplets (Figure S8A–H, Supporting Information). An anti-HLA1 immunotyping of cells in the defect showed that cells inside the osteoid pockets were human and therefore originated from the encapsulated HDF cells

(Figure 8H). Moreover, an estimated 40% of the cells surrounding the pockets contained pluripotent cells with positive Nanog marking (Figure 8H). As to be expected, HLA positive cells were clearly labeled in the HDF only droplets (Figure S8C, Supporting Information), and the SMC + HDF droplets (Figure S8H, Supporting Information), but absent from the SMC only droplets (Figure S8G, Supporting Information). However, endogenous mouse cells and tissues amassed large volumes of repair and regeneration highlighted by the absence of HLA-1 staining in large parts of the defect zone.

The mm-sized fused droplets delivered the HDFs, reprogrammed HDF cells, and a population of differentiated PSCs,
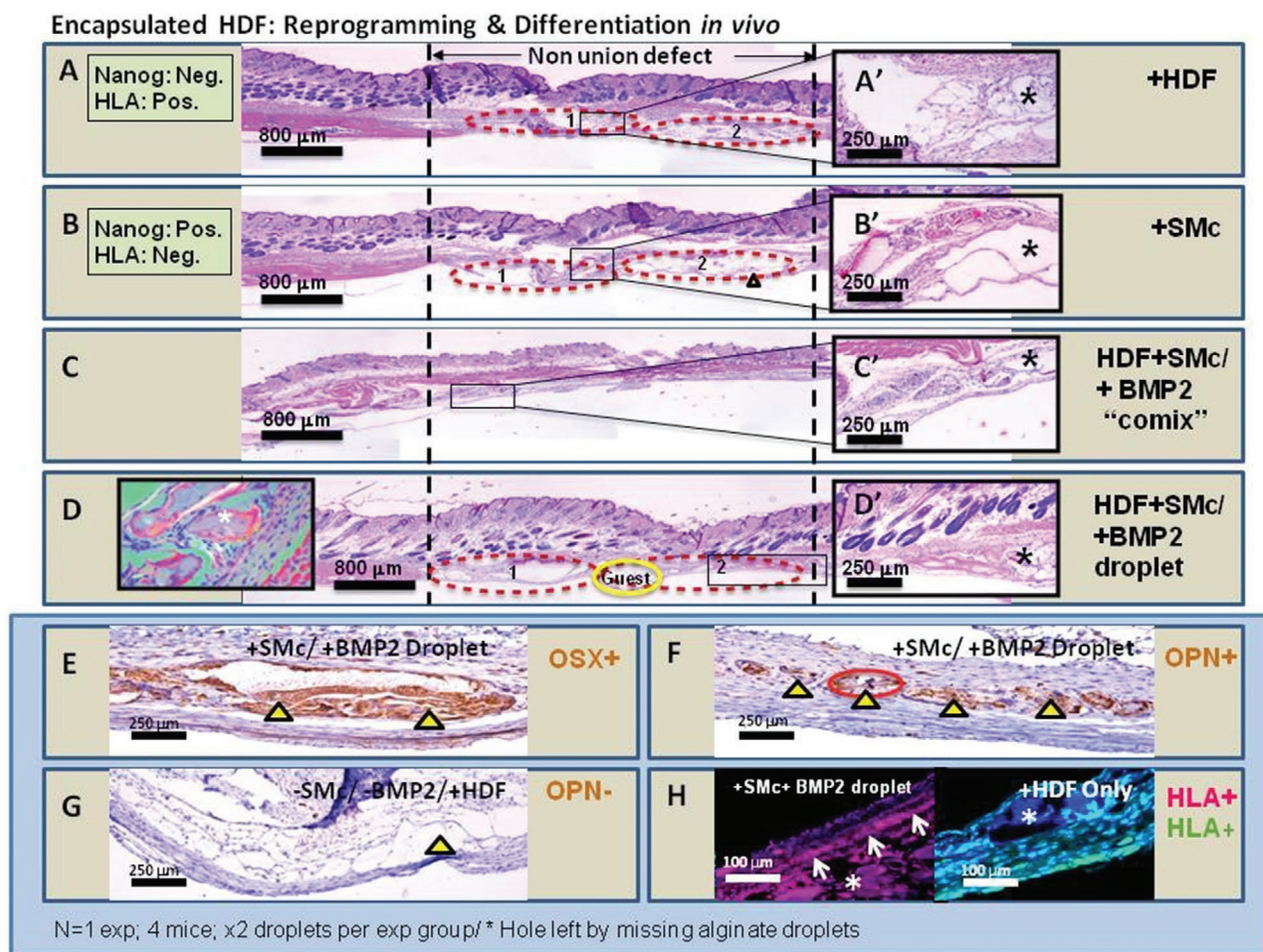
Figure 8. The in vivo interconversion of HDFs into mineralized bone tissue within a cranial defect using SMC/DF loaded alginate-ECMp mm-sized fused droplets. A–H) Histological sections across the calvaria defect infilled with two-time HDF mm-sized fused droplets (with ≈90 000 cells per 14mm³ droplet, inserted manually) after 4-weeks; A) It contains 2 HDF droplets without SMC; A') High magnification (×50 Mag) panel of the outlined area in (A); The images in (B), (C) and (D) correlate to the successive generational stages of osteoid formation, beginning with cellular aggregation into highly structured morphologies; (B) It contains SMc droplets only; B') Highly magnified (×50 Mag) panel of the outlined area in (B). C) Contains mixtures of RPF and DF inside the droplets, showing more re-shaping and densification. C') High magnification (×250) panel of the outlined area in (C); D) SMC droplets (×2 per defect marked with number 1 and 2) each with a nested BMP-2 guest droplet. A solid uniform structure that becomes mineralized is also evident. The left inset shows the polarised light microscopic image of the alginate ignited bone segment. (D') The magnified area in the rectangle at the right side of the droplet 2. E) Osterix (Sp7) positive (OSX+) new tissue formation, existing where the alginate droplets were initially positioned, highlighted by the yellow triangles. (E) Histological section through transplanted droplets containing small molecule compounds and a nested droplet of BMP-2 showing strong expression of OSX. F) A string (highlighted by the yellow triangles) of osteoid pearls defined by positive osteocalcin (OCN) staining; G) OCN staining of the negative control defect without SMC and BMP-2 (yellow the triangle points to the location of pearl clusters of positively stained cells); H) HLA-1+labeled cells across the defect zone in SMC laden droplets (left: HLA = red channel) and HDF cell droplets without SMC infusion (rights: HLA = green; related to A). The red dotted lines (in (A), (B) and (C)) drawn around the implanted alginate fused droplets. The yellow circle (in (D)) outlines an empty guest droplet that remains. The black (A', B,' C' and D') and white (H) stars denote positions of a single droplet.

characterized by Nanog and Sox2 positive labeling into the defect in condensation (Figure S8I–P, Supporting Information). These also delivered small, sporadic groups of HLA+ cells, hence the positive staining positioned in the dermal region and at the interface with brain tissue. HLA+ cells concentrate in the areas of alginate-ECMp and the midline of the reparative tissue running along with the entire defect (white arrows in Figure 8H (left)) and similarly for HDFs in untreated droplets (Figure 8H (right)). The slightly inconsistent resorption, so characteristic of alginate-ECMp in the form used, leads to the untidy cell distribution of the ejected cells. These ejected cells are in the defect and wound site boundaries only. In short,

the droplet types, HDF only, HDF+ BMP-2 and BMP guest droplet developed increasing maturity of the primary sequence of bone formation from cell aggregation into defined shapes, ECM fabricated and well organized mineralized osteoid lined by osteoblasts.

3. Discussion and Conclusions

The study aimed to show the feasibility of the nested droplet system for automated and controlled reprogramming of a standard human somatic cell population and onward

differentiation into specialized cells capable of forming a properly organized tissue.

The technique was rapid, taking 7 days to fully complete. The level of reprogramming was ≈25x higher than the majority of experimental 2D gene integration protocols and the results from applying the Yamanaka assortment of transcription factors to the cells. Moreover, reprogramming was significantly higher than commercially available methods for producing iPSCs. They vary between 0.1% and 1% efficiencies (integrating free techniques: RNA (1%), SeV (0.1%), Epi (0.01%), and Lenti (0.5%) reprogramming methodologies.[51] A few recent reports have shown superior reprogramming efficiencies of 80%.[14]

Polysaccharide-based microenvironments provided the conditions for the consecutive reprogramming of somatic cells and differentiation into new specialized cells within twelve days. The alginate-ECMp matrix entrapped small mobile proteins <20 kDa, adsorbed and trapped in the nanopores (Figure 4F,I; Figure S4A,C, Supporting Information) and passively supported their diffusion throughout the host bead by the work of concentration gradients. The ability to compartmentalize the DF's and the cells inside single and double nested mm-sized fused droplets embedded in a single host framed the scheduling of DF peak exposure time following the measured 23–25% rate of cell reprogramming (Figures 1A, 2C, and 3D). Therefore, we have within a single alginate-ECMp nested module an automatic process of trans differentiation between two individual somatic cell types, via a pluripotent phase, driven by natural forces of diffusion for both small molecules (900 Da on 1 nm-sized intracellular processes) and small differentiation proteins (<70 kDa).

The fraction of transformed cells generated in droplets was on average, ≈25%. As shown, the droplets maintain high viability of 90–95%, particularly in the ultrapure alginate biomaterial. In 1 mL of prepared alginate containing 500 000–2 000 000 somatic cells (fibroblasts), an average of 125 000–500 000 were reprogrammed and differentiated using the nested droplet arrangements. During the cultivation period of 2–4 weeks, we could expect 10–12% cell death (reduced to <5% with ultrapure medical-grade alginate), thus 112 500–450 000 cells available for therapy or tissue engineering. In a typical therapeutic application for tissue engineering, as opposed to stem cell or therapeutic cell delivery to a targeted focus of tissue, the number of functional therapeutic cells required would be >1 billion,[3] meaning that we would require 40 mL of cell-laden alginate at the moderate cell density (2×10^6–1×10^6 mL^{-1}) used throughout this study. This is an excessive bulk volume of biomaterial depending on the application for many tissue engineering applications, where such volumes are absolute for many tissue engineering applications, except for orthopaedics. In practice, roughly calculated, small volumes of new bone, de novo, were generated inside the cranial defect with a total calculated volume ≈39.26 mm^3.

We calculated that a quarter of the treated somatic HDF's was hiPSC reprogrammed. Cells released from mechanical induced spheroids or ELB's after 7 days of small molecule reprogramming (25.2%) formed clones in 2D culture and fully expressed Sox-2 and Oct3/4 pluripotency markers. Interestingly, the HDFs and maintenance of hiPSCs and differentiation occurred in suspension in small 20–100 clusters (and single

cells at 30%) rather than the standard in vitro embryoid bodies, typically an aggregation of between 500–4000 cells.[35]

Additionally, the calculated levels of reprogramming were constant in droplets between 3–8 mm in diameter. While these programming efficiencies are relatively high, but they do not attain levels of 70–80% reported in a few other studies; although still very advantageous. The advantage is threefold: 1) speed, 2) autonomy, 3) arrangement of cells in 3D.

Interestingly, in vivo, the transplanted cells rarely observed instability in the sense of tumorigenicity pertains to media overlying monolayer cultured cells.[51] They generated miniature ovular areas (250 to 300 mm × 100 mm) of developing and fully grown osteoid (nonmineralized bone tissue), running edge-to-edge (Figure 8D–H) along with the 5 mm defect and 250 mm to 800 mm (transverse) × 90 mm (anterior to posterior plane) pockets of mineralized bone, originating inside the droplet fragments of incompletely resorbed mm-sized fused droplets (Figure 8D). The surface areas of bone-like anatomical structures in the +SMc and comix droplets are significantly smaller at ≈80 mm. The in vivo results confirmed our hypothesis that compartmentalization and sequencing accelerate and maximize tissue genesis de novo compared to systems in which the various components mix. The in vivo results confirmed our hypothesis that compartmentalization and sequencing accelerate and maximize tissue genesis de novo compared to systems in which the various components mix.

One of the significant issues is the apparent existence of 75% remaining fibroblasts following both reprogramming and differentiation phases. How do we clear out fibroblasts from the system? Through diffusible factors that target the fibroblasts? Or do we need to immobilize them? Clearly, in vivo, the presence of disproportionate numbers of fibroblasts did not conflict with the essential capacity of droplet differentiated PSC's to generate newly found tissue. Internal droplet microenvironments need to select out PSC's and their progeny against the remaining un-reprogrammed fibroblasts.

The controlling and regulating factors contained within the system at origin and consist of diffusion regulated by the pore structure (at nano- and microscales) minorly contributed by swelling) and semi-permeable diffusion barriers of the structures combined with tensional forces provided by the matrix, hydrostatic pressure, and the stochastic behavior of the cells themselves. In terms of temporal control of the cells to molecular inducted triggering and activation, diffusion is a fundamental driver. The measured rates of protein diffusion in media were paced as such to provide encapsulated cells with functional quantities of cell transformation proteins for differentiation and reprogramming within a cell primed time frame. In all, fine tuning of DF protein signal evolution in time and droplet space is controlled by multivariate characteristics of the alginate gel, the chitosan-alginate polyelectrolyte complex and calcium phosphate infused chitosan membrane at nano, molecular and mesoscales (Figure S9, Supporting Information). We have the four parameters of the polymer determining swelling and diffusivity through the polymer strands together with electric charge, pH, and salt concentrations. The mechanical (strong enough to manipulate and implant) and degradation (droplets begin fracturing and reswelling at 12–14 days) characteristics were reasonably acceptable for short-term- (7–14 days)

cell conversion and growth as well as tissue engineering applications. Further work modulating the properties and parameters of the system to control the time and space evolution of the conversion factors and cell supporting factors augmenting the base alginates and chitosans is required.

We envisage introducing protocell entities as a new variety of nested microdepot (e.g., synthetic cells with lipid membranes and cell mechanics) containing the various DF's, which possess the more precise and complex timepiece mechanics needed for more complex timing operations. Progress toward optimization and honing the system architecture to maximize the transformation efficiency, speed, reproducibility, and tissue-engineered products into well-functioning living tissue modules can only emerge by testing the combinations of parameters on a large permutation grid or a microarray and by manufacturing droplets via microfluidics that differ widely in size, composition, and interactivity. Microfluidics is also more effective at nesting arrangements and adding further shells and layers to the droplets, which also provides additional functionalities in aspects of reaction chemistry and the physical and mechanical properties of the droplet biosystem. Consequently, we shall proceed in this direction by engineering droplet-based microfluidic glass capillary networks for emulsions[51–56] and microemulsions to mechanize the nesting of mineralized polysaccharide mm-sized fused droplets with conceivable diameters varying between 10 and 250 µm and with different contents. Also, to increase the permutations of bead encapsulates and bead microenvironments having a range of chemical, mechanical, and physical properties. This could further maximize cell programming and differentiation.

The material parameters of stiffness, viscoelasticity, strength, hydrostatic pressure, porosity, and others can be easily modulated and fine-tuned in the alginate-ECMp and the alginate-chitosan duplex by cross-linking with PEG and modifying MW, ion and salt concentrations for example.[18] Bare alginate does not have the range of properties for all these material parameters. Instead, alginate combines with another polymer network (e.g., the interpenetrating polymer networks (IPN's) and inorganic 2D lattices) to enhance the mechanical properties and viscoelastic and poroelastic responsiveness, and be decorated with more complex topological arrangements of the polymers, and the density, and distribution of the cellular receptors and integrins throughout the matrix. For example, the matrix stiffness adjusts itself chemically by divalent ion concentration, crosslinking molecules, molecular weight, and others. Similarly, the matrix viscoelasticity can be specified by selective cross-linking, the interpenetration of another polymer network, molecular weight, and quantity of cross-linker to affect relaxation times.[46] Swelling is counteracted in the membrane bound droplets and diffusion occurs at low rates compared to bare alginate, collagen and PEG gels.[43]

These properties define themselves according to the limits that maximize the power of pluripotency induction and later, onward differentiation. The next phase is to trace the process, following transplantation, and confirm that the tissue generation of a defined anatomical structure and function is possible in an animated physiological system.

Another essential purpose for the mm-sized fused droplets is to scale-up the production of therapeutic pluripotent and somatic cells into clinically usable cells, in the many billions, without tumorigenicity and immunogenicity, reviving the wellbeing of millions of future patients.[3] This would require automated synthesizers, fabricators, and generators of the nested droplets, such as a microfluidic device. It would require the development of an injectable applicator and the development of an alginate biomaterial with specific character and behavior mimicking the host tissue, achievable by mathematical modelling of the chemistry and screening of best candidate materials and the encapsulated biomolecules. The properties would need to vary significantly across printed droplet spotted arrays. Thus far, we have yet to test the capability to transform other high availability cell candidates such as adipose cells. Also, the cells can release from bursting droplets (Figure S3, Supporting Information) induced forcibly or spontaneously by ionic and pH changes within the media for experimental investigation and the expansion of iPSC populations (and the selection out of fibroblasts) in plates and flasks.

Another major problem to be tackled is how to stop tumorigenesis activity among the PSC's with their robust self-renewal capability; that is, the unrestrained proliferation of PSC's in the drops and in vivo. Further work is required to optimize not only the droplet production process into droplets with complex compartmentalization but also the concentrations of the RPF, the DF's and ECMp's for specific therapeutic cellular products and the host tissue environment. The modular mm-sized fused droplets serve as a basis for future 4D biomaterials that sequence embryonic and regenerative interactions (we only demonstrated a few including mechanical, small molecules and small protein interactions) in nature-realistic 3D space.

4. Experimental Section

Alginate-ECMp and Chitosan Materials: Protanal© alginate-ECMp powder (CR8223) from Novamatrix (FMC Pharma grade) was the base material for the hydrogels. The alginate-ECMp was relatively pure with an absence of *Salmonella, S. aureus, E. coli, P.aeruginosa* and *Coliform* in the quantities used and some lead (5 ppm), iron (5 ppm), and arsenic (1.5 ppm) contents. The alginate-ECMp consisted of sequenced mannuronic and glucuronic acid residues in a 65 M/35G ratio producing a molecular weight ranging between 250 and 350 kDa. The G-blocks were involved in crosslinking with divalent cations and the selected composition.[48] Reports show that high mannuronic acid sugar (M) alginate-ECMp's do not invoke an immunogenic reaction; thus, the alginate-ECMp hydrogels were made by dissolving the powder in filter-sterilized human iPSC media at 2%, 3%, and 5% w/v. The choice of alginate weight percentages for the solutions was predicated on previous quantities in the alginate literature with a set maximum of 5% representing the threshold where cell viability starts to decrease because of diffusion limitations significantly. The 2% alginate concentration was the minimum density where self-supporting gels form a stable structure. Before contact with living cells, the alginate-ECMp solution was filter sterilized. Chitosan powder (deacetylation degree = 95%) was purchased from Heppe Medical Chitosan GmbH, Germany. A 2% chitosan solution (>7 mPa) was prepared in distilled, filter-sterilized water and again filter sterilized before use to remove the possible contaminants (Pb, Hg, Cd, As), including residual bacteria (<1000 CFU g^{-1}). Previously, the relatively low pH (<6 for proper protonation of the chitosan) of the chitosan solution does not detrimentally affect the cells in close vicinity or contact with the solution for a short time.[30]

HDF Cell Culture: A small-molecule mechanical and chemical dedifferentiated a proprietary human fibroblast cell line (Seoulin

bioscience co, Gyeonggi-do, Korea) led reprogramming kit named, Programin(R) (mciPSC) (Stapworks(R) Stem Cell Limited, Hong Kong) according to the instructions. A single petri-dish contained 3 million to 4 million cells at 90% confluence for each treatment; for individual experiments—the passage number of cells varied was 19–27 at the start to the end of the study, respectively

Small Molecule Transformation of HDFs into hmciPSCs: The Programin(R) (mciPSC) reprogramming kit contains a tri-series cocktail of small molecules (labelled as P1, P2, and P3, manufactured from eight individual purine structures) for the pluripotency conversion of human fibroblasts in a specially prepared media supplemented with nonessential amino acids (X1), GlutaMAX (X1) and sodium pyruvate (X1) and 5% filtered FBS. The small molecules were chemical compounds with eight formulas and structures that vary around the purine group of molecules. In combination, the eight purine derivatives induce the expression of the primary pluripotency genes: Oct3/4, Sox2, and Nanog by 25–100 times that of untreated cells. The kit contains a 96-well plate with each well coated with a superhydrophobic membrane. The fibroblast ESC media suspension was added to 96 wells at a density of 1×10^4 with a media change at 4-days. At seven days, the now reprogrammed spheroids/ELB deposit into small petri dishes, which grew to confluence after a further seven days of culture.

Fabrication of the Differentiation Causing mm-sized Fused Droplets: Guest mm-sized fused droplets (2–3 mm) contained DF's for the onward transformation of hPSC's into representatives of the three germ layer cells and osteogenic cells: Activin A (32–105 kDa), FGF (18 kDa), EGF (6.4 kDa), Retinoic acid (0.3 kDa), bFGF (18 kDa), BMP-4 (13 kDa), and Wnt3a (37.4 kDa; StemPro Differentiation kit, R&D Systems, Minneapolis, MN, USA). Below is a table listing the various morphogen combinations for ectodermal, endodermal, and mesodermal cell induction.

All of the factors were at sizes that could diffuse through the alginate-ECMp nanopores (40–60 nm) and the chitosan/calcium phosphate (CaP) semipermeable membrane with much smaller nanopores of 50–250 nm (Figure S3A–C, Supporting Information). Mm-sized fused droplets of alginate-ECMp solution containing the DF's, at specified concentrations, optimized for media overlying a continuous monolayer of plated cells (StemPro Differentiation kit, R&D Systems, Minneapolis, MN, USA), were added to the chitosan solution and incubated therein for either 30 or 60 min to generate two mm-sized fused droplets. The droplets bore 2x or 3x the stiffness of the host droplet. The 30 min formed droplet was designed for the one time delivery (single nested droplet system) of DF's and the 60 min formed droplet engineered for the second droplet (the one designed to release its contents by diffusion after the first droplet, so in a sequence), in the double nested droplet arrangement, that delivers a second round of differentiation factor diffusion to the host cells.

Preparation of Cell Adhesive Alginate-ECMp mm-sized Fused Droplets and Cell Encapsulation: Sodium alginate-ECMp powder was obtained from FMC biopolymer (Protanal CR 8223 (Pharma grade >900 mPa; M/G ratio = 65/35; 300 kDa M_W)) and Arcturus (as alginic acid powder) and reconstituted at 2% w/v. in DMEM/F12 media (GibCo) containing Programin(R) (mciPSC) component 1 (1×10^{-3} м), component 2 (3 µM), component 3 (4 µM) 1X GlutaMAX (GibCo), 1X NEAA (GibCo), 1X Sodium pyruvate (GibCo) and 0.1×10^{-3} м β-mercaptoethanol, the differentiation protein cocktail media, and the Programin(R) (mciPSC) the 1, 2 numbered, Programin 1 and 2, nonprogramming media formulations representing the specific admixtures of the eight purine compounds. The full reprogramming media contained Programin 1,2 and the active cocompound, Programin 3. Alginate-ECMp-Programin (mciPSC) solutions suspended 80–110 000 fibroblasts per droplet (3000–8000 µm with volumes of between 14 and 268 mm³)) in different compositions so that they were dissociated in the alginate-ECMp matrix singly and in small clusters (≈20–250+ cells). The mm-sized fused droplets were synthesized and assembled through nesting and multiple nesting according to a previously published method.[30]

Preparation of GRGDSP-MVG (NOVATACH) Alginate for Cell Encapsulation in the Droplets: A 100 mg lyophilized sample of peptide coupled alginate (NOVATACH, Nova Matrix, FMC, AS, Sandvika, Norway). This was ultrapure alginate (no impurities that affect living cell metabolism, function, and health) lyophilized solid with a high G and a high MW (G/M Ratio: ≥1.5)). The ultrapure alginate bears the cell adhesive tripeptide RGD ((G) and (DSP) were spacers, chemically conjugated to the polymer backbone) was thoroughly mixed with 5 mL of ESC media for two hours and prepared. This alginate possessed a precisely engineered configuration of M and G sugars along the alginate polymer chain, which optimizes the alginate hydrogel with high degrees of cell interactivity.[48] Cell adhesion ligands increase cell attachment to the biopolymer matrix and boost cell productivity.

ECM Augmented Alginate-ECMp Material for Cell Adhesion and Organization: Cell interactivity of the alginate-ECMp framework improved by adding essential human ECM cell binding components-principally representatives of the basement membrane (BM). Nanogram concentrations of laminin (0.3 mL per bead; derived from human placenta tissue) and collagen IV (0.3 mL per bead; from the human placenta), chondroitin sulphate (shark cartilage; 0.12 mL per bead) and RGD tripeptides (0.1 mL mL⁻¹ GRGDS, Sigma)[7] which infuse into the alginate-ECMp solutions in making all the mm-sized fused droplets except for the intended differentiation mm-sized fused droplets, which inserted into the primary reprogramming host.

Comixed Alginate-RPF and DF Droplets: Alginate solution, made-up of from ESC media mixed with the highly selective ECMp's, the small molecular RPF's dissolved in the media at mM concentrations and liquid DF's (ng concentrations; refer to **section 5.1.4**) at the optimal concentrations for plated cells in a monolayer according to Yang et al. 2004[57] for BMP2 effectiveness on multipotent stem cells and the germ layer cells, differentiation according to the instructions laid out in the StemPro differentiation kit protocol. The super mix of alginate was added dropwise into the chitosan solution to create fused droplets as previously described.

Assembly of Nested Polysaccharide mm-sized Fused Droplets: Spatial and temporal separation (*i.e.*, the manufacture of diffusion barriers for the control of DF dispersal) was engineered by creating nested arrangements of mm-sized fused droplets. Pushing the smaller, stiffened 0.5–2 mm guest into the soft, minimally cross-linked 3–8 mm alginate-ECMp droplet, immediately following the suspension in the chitosan solution $(C_6H_{11}NO_4)$n with 70% of the polymer strands containing free amino acids; Heppe Medical Chitosan GmbH, Germany), carried out nested arrangements of 0.5–2 mm guest droplets inside a 3–8 mm host. The host remains soft and deformable to stiff mm-sized fused droplets. During the insertion, imperceptible quantities of encapsulates were released from the soft host as the insertion action was instantaneous, lasting a matter of a few seconds. This fact was demonstrated in experiments using a red dye. Breakage of the membrane in chitosan solution draws in replacement chitosan at the interfacial wound site, and reassembly of the membrane occurs by a return of electrostatic reactions. The chemical composition of small guest bead cores and the shell were tailored to reduce permeability (alginate-ECMp nanopores) and to increase thicknesses.

Nested Droplet Diffusion Experiments: In the first bead-in-bead transfusion experiments, the guest mm-sized fused droplets were loaded with a hematoxylin dye and inserted into a host. The dispersal of the colorimetric dye between the guest and the host mm-sized fused droplets was tracked day-by-day for 7–10 days. It was then proceeded to monitor the movement of entrapped FITC labelled dextran's with particle sizes of 10 000 M_W and 70 000 M_W (Sigma-Aldrich), matching the upper and lower size range of growth factors and the DF's. To do this, the FITC intensity of the suspension was measured by spectrophotometry, in addition to CLSM measurements of fluorescence at a 555 nm excitation by the image analysis software. Capsules were produced with a predetermined range of membrane thicknesses (11–60 µm) and permeabilities by adjusting the concentration of calcium chloride (5×10^{-3}, 15×10^{-3}, 25×10^{-3}, and 50×10^{-3} м), sodium phosphate (100×10^{-3} and 200×10^{-3} м) and times for hardening (10, 20 30, and 60 min)

**ADVANCED
SCIENCE NEWS**

www.advancedsciencenews.com

**ADVANCED
BIOSYSTEMS**

www.adv-biosys.com

for interfacial precipitation and densification of semi-crystalline calcium phosphate.

Nested Droplet Diffusion Experiments—Coupled Induction and Differentiation Inside Nested Alginate-ECMp mm-Sized Fused Droplets: The spatial separation of the factors scheduled the accelerated transformation of HDFs to endodermal, ectodermal, and mesodermal germ cells or osteoblasts. The alginate-ECMp hydrogel was 95% water and possesses 40 nm pores, facilitating diffusion in all directions throughout the host bead, considering the MW of most small molecules were less than <900 Da and act in the 1 nm range. Besides, DF mm-sized fused droplets were suspended in the media, also containing HDF filled Programin (mciPSC) mm-sized fused droplets.

Nested Droplet Diffusion Experiments—Animal Ethics: The animal experiments had approval from the Yonsei University Health System Institutional Animal Care and Use Committee (YUHS-IACUC) following the Guidelines for the care of small laboratory animals (National Research Council, United States). The YUHS-IACUC committee gave permission, and the experiments agreed to the rules of their decision.

Nested Droplet Diffusion Experiments—In Vivo Transplantation of Regular, Programin [SMc] (mciPSC) and Nested DF Containing mm-Sized Fused Droplets: Three-week-old nude mice (all males) came from KOATECH (Pyeongtaek, Korea) and prepared individually for the bone defect model and the subcutaneous pocket. The invasive surgical operations were carried out under anaesthesia in a total of 15 individual mice with 5 mice used for the cranial defect model and 10 mice for the subcutaneous pocket trials. The multiple nested droplets were transplanted into a 5 mm calvaria nonunion defect of immunodeficient mice for up to four weeks to highlight the de novo bone formation capacity. Modules for germ-layer differentiation were implanted in a subcutaneous pocket on the lower flanks of nude mice and removed at two weeks to offset tissue blanketing. The calvaria defect zone was demineralized and fixed in 4% PFA. Histological thin (7 mm) sectioning examined the characteristics of cell transformations and the tissue amassed from cell growth and development in response to the varied alginate-ECMp microenvironments. Sections stained for standard immunolabeling protocols.

Nested Droplet Diffusion Experiments—Immunolabelling of Cell Surface Markers and Transcription Factors: Antibody labelling distinguished the identity of HDF cells for the expression of SMA and Vimentin. Positive labelling for the following human pluripotency markers designated cell pluripotency: TRA-1-81, Sox-2, SSEA-4, Oct3/4, Nanog, SSEA-1, and TRA-1-61 (StemLight Pluripotency Antibody Kit #9656, Cell signalling technology).Differentiated PS cells marked for the three germ layer lineages using: Goat Anti-Human Otx2 Antigen Affinity-purified Polyclonal Antibody, Goat Anti-Human Brachyury Antigen Affinity-purified Polyclonal Antibody, and Goat Anti-Human SOX17 Antigen Affinity-purified Polyclonal Antibody. HLA class 1 antibody (Abcam ab70328) was applied to in vivo sections to distinguish implanted human cells and their contribution to tissue formation.

Nested Droplet Diffusion Experiments—Marking mciPSC with Stem Cell Dye (108) and Lectin Molecules: The ESC 108 stem cell dye was a Rhodamine molecule ($C35H46CIN3O3$) that distinguishes live human hESC's and induced hPSC's, but not fibroblasts. The dye molecule strongly associates with the Rsp8 protein component of the ribosomal 40S subunit located inside the nucleus. The lectin molecule UEA-1 engages and docks with its complementary carbohydrate motif pieced within the cell glycocalyx specifically expressed by ESC cells. Streptavidin was bound to the biotinylated lectin, and a coating of biotinylated alginate-ECMp overlaid the lectin-biotin-streptavidin complex. On top of that, chitosan infused with Rhodamine dye and bound into the alginate-ECMp coating by electrostatic attraction.[32] Thus, successful lectin binding onto the ESC-like cell membrane interface results in the double coating and the existence of the rhodamine fluorescence.

Nested Droplet Diffusion Experiments—Marked Cell Counting in Fluorescent Images by ImageJ software: Labelled cells were counted from in situ images of HDFs, hPSC's and differentiated phenotypes expressing Sox-2, Oct 3/4, Osterix, SMA, Runx-2, Brachyury, Sox 17, Nanog, and Otx-2. Percentages of the different phenotypes calculated between green

and red marked cells and unmarked cells showing only the DAPI nuclear counterstain to determine the relative efficiencies of reprogramming and differentiation in 1280 × 1280 mm pixel space (n = 12). A sequence of six options, featured in FIJI, enabled the red, green and blue colours to be manually selected: PLUGINS>>>ANALYZE>>>CELL COUNTER>>>Initialize>>>Counters.

Nested Droplet Diffusion Experiments—FACS Analysis of Reprogrammed and Differentiated Cells: HDF cell-alginate-ECMp mm-sized fused droplets were dissolved in 0.2×10^{-3} M sodium citrate (Sigma) for 12 h to overnight. hPSC's were harvested and aliquoted at 1×10^6 cells per mL. Human mciPSCs were fixed in 4% PFA for 10 min at 37°C. The cells were then washed with PBS 3 times over, each lasting 5 min. Next, the cells were blocked in 0.5% BSA for 30 min. Anti-Nanog and Runx-2 Abs were incubated with hPSC's for 1 h at room temperature. Further triple washing of the cells in PBS before applying the secondary antibody. Again, the cells were incubated for 1 h at room temperature, followed by three consecutive PBS washes. A BDSII flow cytometer undertook cytometric measurements.

Nested Droplet Diffusion Experiments—RT-qPCR Gene Expression Analysis: Cells were released from mm-sized fused droplets by first immersing them in Trizol solution and vigorous mechanical scraping for 10 min. The cells in suspension were removed from the solution by centrifugation and processed for the extraction of RNA using the standard chloroform-isopropanol based protocol ending in the dissolution with RNAse water. Spectrophotometric absorbance measurements of the sample to check for quantity and quality before the conversion to cDNA were processed using the Maxime RT PreMix (OligodT primer) kit purchased from iNtRON Biotech Inc. The RT-PCR used a Thermal Cycler Dice TP600 (Takara, Japan) with AccuPower PCR PreMix (Bioneer, Korea), and amplification occurred after 40 cycles. RT-qPCR analyzed the transcripts of Nanog, Sox-2, Klf4, Oct3/4, and FGF-4 in triplicate (the primers for this reaction came from GenoTech Corp, Daejon, Korea. GAPDH housekeeping gene counterbalanced the quantity of each gene. RQ results for the re-programmed HDF's in mm-sized fused droplets were presented as bar graphs contrasted against the untreated control group and FGF-4 marker for the remaining unprogrammed HDFs. The primer sequences selected and used for the PCR analysis are listed below as follows:

Human primer sequences

GAPDH:	Forward	GAA GGT GAA GGT CGG AGT CA
	Reverse	TTG AGG TCA ATG AAG GGG TC
Oct 4:	Forward	AAG CTC CTG AAG CAG AAG AGG ATC ACC
	Reverse	GTT CAT AGA ACC ACA CTC GGA CCA CAT
Sox 2:	Forward	GGA AAA CCA AGA CGC TCA TGA AGA AGG
	Reverse	GTT CAT GTA GGT CTG CGA GCT GGT CAT
Klf4:	Forward	AGA GTT CCC ATC TCA AGG CA
	Reverse	GTC AGT TCA TCT GAG CGG G
Fgf4:	Forward	GAT GAG TGC ACG TTC AAG GA
	Reverse	GGT TCC CCT TCT TGG TCT TC
Nanog:	Forward	CCT CCA TGG ATC TGC TTA TTC AGG ACA
	Reverse	CCT TCT GCG TCA CAC CAT TGC TAT TCT

Nested Droplet Diffusion Experiments—Mathematical Calculations of Alginate Hydrogel Behavior in the Solvent Diffusion: The behavior-mechanical, physical, and diffusivity was predictable using mathematical modelling equations, as recently described by Caccavo et al.[46] The calculus was used to determine the behavior of the solvent (ESC media carrying the DF's) through the alginate hydrogel and predicted its general materials behavior. A fine selection of the viscoelastic and poroelastic properties was vital for engineering good cell compatibility and tissue engineering outcomes. Mathematical equations build models that can predict individual properties from basic characters of the

material for synthesis. Caccavo et al. published the relevant models.[46] A simple model was used to predict the viscoelastic and poroelastic properties of the materials, which was not measured after fabrication, used in reprogramming and onward differentiation.

The following parameters were needed to be calculated:-

t_D = diffusion time, which was calculated by, t_D = LCH2/D
t_R = viscous relaxation time
t_P = process time
Lch = length of diffusion

Droplet Swelling Characteristics: Polysaccharide droplets were fabricated conventionally using a previous published method.[30] The droplets were washed in PBS to clear away any residual chitosan. After droplet formation, the droplet size was measured. The swelling was measured by dilation rather than by weight. Next, media immersed droplets for up to 14 days. On each day, the droplet diameter was measured. Any swelling would be identified by the change in the diameter of the droplet due to swelling. A graph of droplet enlargement was plotted over 14 days.

Release from the droplet and hence diffusion force and the rate are summarized by $M_t/M\infty = kt^n$

Droplet Swelling Characteristics—Molecular Diffusion through Alginate Hydrogel: Small channels measuring 1 mm in diameter were etched into a cutaway section of a compact disc. These channels were then infilled with alginate solutions from one end to the other with a syringe. The plastic disc piece was immersed gradually in chitosan solution to both crosslinks and solidify the alginate ionotropically, through chain entanglement and electrical charges between alginate and chitosan polymer chains. Small molecules were coupled with a natural dye to visualize the spatial distribution of diffusion over the 14 days.[58]

Egg yolk phosvitin, which was 35 kDa was mixed into the chitosan-coated alginate cylinders placed inside the apparatus and the yellow color was traced through over 7 days.

Droplet Swelling Characteristics—Nested Biomolecule Release: New experimental evidence bolstered the idea that nested droplet containment of biomolecules slowed down the external release of encapsulated biomolecules. Experiments measured the quantity of 1% tyrosinase eluted from nested droplets to the external environment after 48 and 144 h (Data not shown). UV/Vis detected tyrosinase (120 kDa) quantity at 280 nm at the two-time points. Single nested beads slightly delayed the enzyme released compared to tyrosinase encapsulated in one bead only. A significant delay occurred in the double nested tyrosinase arrangement. The difference between the one nested and two nested based tyrosinase release systems was not proportionate.

Droplet Swelling Characteristics—Physical and Chemical Parameters to Describe Hydrogel Structures and Properties: Significant microscopic properties of dynamically behaving hydrogel polymers, related to chains and crosslinks, can be calculated using series of mathematical partial differential equations. Usefully, four separate parameters of polymers can be used to calculate probable and partial resolutions of diffusivity, Young's modulus, viscoelasticity, hydration and poroelasticity. The equations were extracted from Caccavo et al[43]

Mesh size: $\xi = l \cdot \phi_{2,s}^{-\frac{1}{3}} \cdot \left(C_n \cdot \frac{2 \cdot M_c}{M_r} \right)^{\frac{1}{2}}$

Mol. Wt. between crosslinks: $\frac{1}{M_c} = \frac{1}{M_n} - \frac{\bar{\upsilon} \cdot [\ln(1 - \phi_{2s}) + \phi_{2s} + \chi_{12}\phi_{2s}^2]}{\Omega_1 \cdot \left(\phi_{2s}^{\frac{1}{3}} - \frac{\phi_{2s}}{2} \right)}$

Mr and length of repeating unit are taken from the literature.

Droplet Swelling Characteristics—Mechanical and Rheological Measures: The mechanical properties and single rheological measurement were calculated from the four parameters described in 5.3.3 and from the literature.

Supporting Information

Supporting Information is available from the Wiley Online Library or from the author.

Conflict of Interest

The authors declare no conflict of interest.

[1] A. B. Cherry, G. Q. Daley, *Cell* **2012**, *148*, 1110.
[2] T. P. Kraehenbuehl, R. Langer, L. S. Ferreira, *Nat. Methods* **2011**, *8*, 731.
[3] A. D. Celiz, J. G. Smith, R. Langer, D. G. Anderson, D. A. Winkler, D. A. Barrett, M. C. Davies, L. E. Young, C. Denning, M. R. Alexander, *Nat. Mater.* **2014**, *13*, 570.
[4] M. Ohnuki, K. Takahashi, *Philos. Trans. R. Soc., B* **2015**, *370*, 20140367.
[5] K. M. Fridley, M. A. Kinney, T. C. McDevitt, *Stem Cell Res. Ther.* **2012**, *3*, 45.
[6] X. Gaeta, Y. Xie, W. E. Lowry, *Nat. Cell Biol.* **2013**, *15*, 725.
[7] D. W. Green, G. Watson, J. Watson, J.-M. Lee, H.-S. Jung, *Adv. Biosyst.* **2017**, *1*, 1700116.
[8] M. P. Lutolf, P. M. Gilbert, H. M. Blau, *Nature* **2009**, *462*, 433.
[9] C. Kropp, D. Massai, R. Zweigerdt, *Process Biochem.* **2017**, *59*, 244.
[10] Z. Tong, A. Solanki, A. Hamilos, O. Levy, K. Wen, X. Yin, J. M. Karp, *EMBO J.* **2015**, *34*, 987.
[11] S. Eminli, A. Foudi, M. Stadtfeld, N. Maherali, T. Ahfeldt, G. Mostoslavsky, H. Hock, K. Hochedlinger, *Nat. Genet.* **2009**, *41*, 968.
[12] K. Woltjen, I. P. Michael, P. Mohseni, R. Desai, M. Mileikovsky, R. Hämäläinen, C. R. W. Wang, P. Liu, M. Gertsenstein, K. Kaji, H. K. Sung, A. Nagy, *Nature.* **2009**, *458*, 766.
[13] K. Takahashi, S. Yamanaka, *Nat. Rev. Mol. Cell Biol.* **2016**, *17*, 183.
[14] F. Chen, G. Zhang, L. Yu, Y. Feng, X. Li, Z. Zhang, Y. Wang, D. Sun, S. Pradhan, *Stem Cell Res. Ther.* **2016**, *7*, 99.
[15] D. Cyranoski, *Nature.* **2014**, *516*, 162.
[16] F. González, S. Boué, J. C. Izpisúa Belmonte, *Nat. Rev. Genet.* **2011**, *12*, 231.
[17] N. Zagris, *Micron* **2001**, *32*, 427.
[18] M. Caiazzo, Y. Okawa, A. Ranga, A. Piersigilli, Y. Tabata, M. P. Lutolf, *Nat. Mater.* **2016**, *15*, 344.
[19] A. Singh, J. Elieseff, *J. Mater. Chem.* **2010**, *20*, 8832.

[20] S. Battista, D. Guarnieri, C. Borselli, S. Zeppetelli, A. Borzacchiello, L. Mayol, D. Gerbasio, D. R. Keene, L. Ambrosio, P. A. Netti, *Biomaterials* **2005**, *26*, 6194.

[21] S. S. Chen, W. Fitzgerald, J. Zimmerberg, H. K. Kleinman, L. Margolis, *Stem Cells* **2007**, *25*, 53.

[22] J. E. Dixon, D. A. Shah, C. Rogers, S. Hall, N. Weston, C. D. Parmenter, D. McNally, C. Denning, K. M. Shakesheff, *Proc. Natl. Acad. Sci. USA* **2014**, *111*, 5580.

[23] D. S. Benoit, A. R. Durney, K. R. Anseth, *Biomaterials* **2007**, *28*, 66.

[24] B. B. Mandal, A. Grinberg, E. S. Gil, B. Panilaitis, D. L. Kaplan, *Acta Biomater.* **2009**, *5*, 2579.

[25] N. Mitrousis, A. Fokina, M. S. Shoichet, *Nat. Rev. Mater.* **2018**, *3*, 441.

[26] J. Utikal, J. M. Polo, M. Stadtfeld, N. Maherali, W. Kulalert, R. M. Walsh, J. G. Rheinwald, K. Hochedlinger, *Nature* **2009**, *460*, 1145.

[27] J. Long, K. H. D. Kim, J. B. Lee, D. H. Kim, *J. Mater. Chem. B* **2017**, *5*, 2375.

[28] N. S. Hwang, S. Varghese, J. Elisseeff, *PLoS One* **2008**, *3*, e2498.

[29] S. Levenberg, J. S. Golub, M. Amit, J. Itskovitz-Eldor, R. Langer, *Proc. Natl. Acad. Sci. USA* **2002**, *99*, 4391.

[30] D. W. Green, I. Leveque, D. Walsh, D. Howard, X. B. Yang, S. M. K. A. Partridge, R. O. C. Oreffo, *Adv. Funct. Mater.* **2005**, *15*, 917.

[31] L. S. Ferreira, S. Gerecht, J. Fuller, H. F. Shieh, G. Vunjak-Novakovic, R. Langer, *Biomaterials* **2007**, *28*, 2706.

[32] J. C. Mohr, J. Zhang, S. M. Azarin, A. G. Soerens, J. J. de Pablo, J. A. Thomson, G. E. Lyons, S. P. Palecek, T. J. Kamp, *Biomaterials* **2010**, *31*, 1885.

[33] A. Mongera, P. Rowghanian, H. J. Gustafson, E. Shelton, D. A. Kealhofer, E. K. Carn, F. Serwane, A. A. Lucio, J. Giammona, O. Campàs, *Nature.* **2018**, *561*, 401.

[34] Y. D. Teng, E. B. Lavik, X. Qu, K. I. Park, J. Ourednik, D. Zurakowski, R. Langer, E. Y. Snyder, *Proc. Natl. Acad. Sci. USA* **2002**, *99*, 3024.

[35] L. Anastasia, M. Sampaolesi, N. Papini, D. Oleari, G. Lamorte, C. Tringali, E. Monti, D. Galli, G. Tettamanti, G. Cossu, B. Venerando, *Cell Death Differ.* **2006**, *13*, 2042.

[36] K. A. Moore, I. R. Lemischka, *Science* **2006**, *31*, 5769.

[37] D. R. Amant, *Dev. Biol.* **2005**, *280*, 260.

[38] K. K. H. Lee, T. L. M. Lo, H. H. Cheung, W. Y. Chan, *US 10676720*, **2020**.

[39] Y. C. Wang, M. Nakagawa, I. Garitaonandia, I. Slavin, G. Altun, R. M. Lacharite, K. L. Nazor, H. T. Tran, C. L. Lynch, T. R. Leonardo, Y. Liu, S. E. Peterson, L. C. Laurent, S. Yamanaka, J. F. Loring, *Cell Res.* **2011**, *21*, 1551.

[40] Y. Leychkis, S. R. Munzer, J. L. Richardson, *Studies in History Philos. Sci. Part C: Studies History Philos. Biol. Biomed. Sci.* **2009**, *40*, 312.

[41] D. W. Green, K. A. Partridge, J. C. Pound, D. Walsh, I. Leveque, R. Tare, S. Mann, R. O. C. Oreffo, *J. Bone Min. Res.* **2007**, *20*, 1300.

[42] J. Oyaas, I. Storrø, H. Svendsen, D. W. Levine, *Biotechnol. Bioeng.* **1995**, *47*, 492.

[43] M. H. Hettiaratchi, A. Schudel, T. Rouse, A. J. García, S. N. Thomas, R. E. Guldberg, T. C. McDevitt, *APL Bioeng.* **2018**, *2*, 026110.

[44] O. Gåserød, A. Sannes, G. Skjåk-Braek, *Biomaterials.* **1999**, *20*, 773.

[45] A. Serrano-Aroca, J. F. Ruiz-Pividal, M. Llorens-Gámez, *Sci. Rep.* **2017**, *7*, 11684.

[46] D. Caccavo, S. Cascone, G. Lamberti, A. A. Barba, *Chem. Soc. Rev.* **2018**, *47*, 2357.

[47] T. Boontheekul, H. J. Kong, D. J. Mooney, *Biomaterials* **2005**, *26*, 2455.

[48] K. Y. Lee, D. J. Mooney, *Prog. Polym. Sci.* **2012**, *37*, 106.

[49] E. Axpe, D. Chan, G. S. Offeddu, Y. Chang, D. Merida, H. L. Hernandez, E. A. Appel, *Macromolecules* **2019**, *52*, 6889.

[50] M. Schuldiner, O. Yanuka, J. Itskovitz-Eldor, D. A. Melton, N. Benvenisty, *Proc. Natl. Acad. Sci. USA* **2000**, *97*, 11307.

[51] T. M. Schlaeger, L. Daheron, T. R. Brickler, S. Entwisle, K. Chan, A. Cianci, A. DeVine, A. Ettenger, K. Fitzgerald, M. Godfrey, D. Gupta, J. McPherson, P. Malwadkar, M. Gupta, B. Bell, A. Doi, N. Jung, X. Li, M. S. Lynes, E. Brookes, A. B. Cherry, D. Demirbas, A. M. Tsankov, L. I. Zon, L. L. Rubin, A. P. Feinberg, A. Meissner, C. A. Cowan, G. Q. Daley, *Nat. Biotechnol.* **2015**, *33*, 58.

[52] L. Hou, J. J. Kim, M. Wanjare, B. Patlolla, J. Coller, V. Natu, T. J. Hastie, N. F. Huang, *Sci. Rep.* **2017**, *7*, 6551.

[53] K. Nishino, Y. Arai, K. Takasawa, M. Toyoda, M. Yamazaki-Inoue, T. Sugawara, H. Akutsu, K. Nishimura, M. Ohtaka, M. Nakanishi, A. Umezawa, *Regener. Ther.* **2018**, *9*, 71.

[54] L. Y. Chu, A. S. Utada, R. K. Shah, J. W. Kim, D. A. Weitz, *Angew. Chem., Int. Ed.* **2007**, *46*, 8970.

[55] C. J. Martinez, J. W. Kim, C. Ye, I. Ortiz, A. C. Rowat, M. Marquez, D. Weitz, *Macromol. Biosci.* **2012**, *12*, 946.

[56] S. Utech, R. Prodanovic, A. S. Mao, R. Ostafe, D. J. Mooney, D. A. Weitz, *Adv. Healthcare Mater.* **2015**, *4*, 1628.

[57] X. B. Yang, R. S. Bhatnagar, S. Li, R. O. C. Oreffo, *Tissue Eng.* **2004**, *10*, 1148.

[58] C. García-Aparicio, I. Quijada-Garrido, L. Garrid, *J. Colloid Interface Sci.* **2012**, *368*, 14.